Astrocytes phagocytose adult hippocampal synapses for circuit homeostasis

https://doi.org/10.1038/s41586-020-03060-3

Received: 8 March 2020

Accepted: 5 November 2020

Published online: 23 December 2020

Check for updates

Joon-Hyuk Lee[1,5], Ji-young Kim[2,3,5], Seulgi Noh[3,4], Hyoeun Lee[2], Se Young Lee[1], Ji Young Mun[4], Hyungju Park[2,3]✉ & Won-Suk Chung[1]✉

In the adult hippocampus, synapses are constantly formed and eliminated[1,2]. However, the exact function of synapse elimination in the adult brain, and how it is regulated, are largely unknown. Here we show that astrocytic phagocytosis[3] is important for maintaining proper hippocampal synaptic connectivity and plasticity. By using fluorescent phagocytosis reporters, we find that excitatory and inhibitory synapses are eliminated by glial phagocytosis in the CA1 region of the adult mouse hippocampus. Unexpectedly, we found that astrocytes have a major role in the neuronal activity-dependent elimination of excitatory synapses. Furthermore, mice in which astrocytes lack the phagocytic receptor MEGF10 show a reduction in the elimination of excitatory synapses; as a result, excessive but functionally impaired synapses accumulate. Finally, *Megf10*-knockout mice show defective long-term synaptic plasticity and impaired formation of hippocampal memories. Together, our data provide strong evidence that astrocytes eliminate unnecessary excitatory synaptic connections in the adult hippocampus through MEGF10, and that this astrocytic function is crucial for maintaining circuit connectivity and thereby supporting cognitive function.

Adult synapses constantly undergo synaptic turnover[1,2] during experience-dependent plasticity and cognitive functions[4–6]. However, it is unclear how synapses in the adult brain are eliminated and whether synapse elimination has a direct role in circuit homeostasis.

Astrocytes eliminate synapses by phagocytosis during postnatal development[3]. By phagocytosing synapses through the MEGF10 and MERTK phagocytic receptors, astrocytes actively contribute to activity-dependent synapse pruning and developmental refinement of circuits. Moreover, contrary to the previous notion that microglia are the sole mediators of synapse elimination[7–9], astrocytes have been shown to have a major role in eliminating synapses in developing brains. On the basis of these findings, we hypothesized that synapses in the adult brains are also refined by astrocytic phagocytosis, and that such elimination is critical for maintaining circuit homeostasis.

Monitoring glial phagocytosis in vivo

We took advantage of an mCherry–eGFP (enhanced green fluorescent protein) reporter system that has been used to monitor autophagic acidification influx[10]. Whereas both mCherry and eGFP maintain intact fluorescent intensities under neutral pH conditions, only the mCherry signal—but not the eGFP signal—is preserved in acidic environments, such as in the lysosome[11]. To test this system for monitoring glial phagocytosis, we first generated adeno-associated virus 9 (AAV9) vectors encoding human synapsin promoter (h*SYN*)-driven membrane-bound (lyn) mCherry–eGFP (Extended Data Fig. 1a, b). When we injected this AAV reporter into the CA3 hippocampus of adult mice, most CA3 neurons and their projections were labelled by both mCherry and eGFP (Extended Data Fig. 1c, d). However, when we examined CA1 regions innervated by CA3 neurons, we found numerous distinct puncta of mCherry alone, indicating that they were inside acidic organelles (Extended Data Fig. 1d). Moreover, most mCherry-alone puncta were in either astrocytes or microglia (Extended Data Fig. 1e).

Notably, injection of the same virus into the lateral geniculate nucleus, to label thalamocortical inputs to the primary visual cortex, did not produce mCherry-alone puncta (Extended Data Fig. 1f–h). These data indicate that, unlike thalamocortical circuits, adult hippocampal CA3–CA1 circuits undergo substantial synapse turnover through glial phagocytosis.

Astrocytic phagocytosis of adult synapses

To directly detect phagocytosis of synapses by glial cells, we designed four additional reporters. ExPre encoded synaptophysin (SYP)–mCherry–eGFP driven by the h*SYN* promoter, to target the presynaptic structures of excitatory synapses. The InhiPre reporter encoded the same fusion protein, driven by the *Gad67* (also known as *Gad1*) promoter to localize it to inhibitory synapses. For postsynaptic structures, we used the h*SYN* promoter to drive expression of PSD95–mCherry–eGFP in excitatory synapses, or of gephyrin (GPHN)–mCherry–eGFP in inhibitory synapses (ExPost or InhiPost, respectively) (Fig. 1a). When we injected AAV9 vectors carrying ExPre, InhiPre, ExPost or InhiPost

[1]Department of Biological Sciences, Korea Advanced Institute of Science and Technology (KAIST), Daejeon, Republic of Korea. [2]Research Group for Neurovascular Unit, Korea Brain Research Institute (KBRI), Daegu, Republic of Korea. [3]Department of Brain and Cognitive Sciences, Daegu Gyeongbuk Institute of Science and Technology (DGIST), Daegu, Republic of Korea. [4]Research Group for Neural Circuit, Korea Brain Research Institute (KBRI), Daegu, Republic of Korea. [5]These authors contributed equally: Joon-Hyuk Lee, Ji-young Kim. ✉e-mail: phj2@kbri.re.kr; wonsuk.chung@kaist.ac.kr

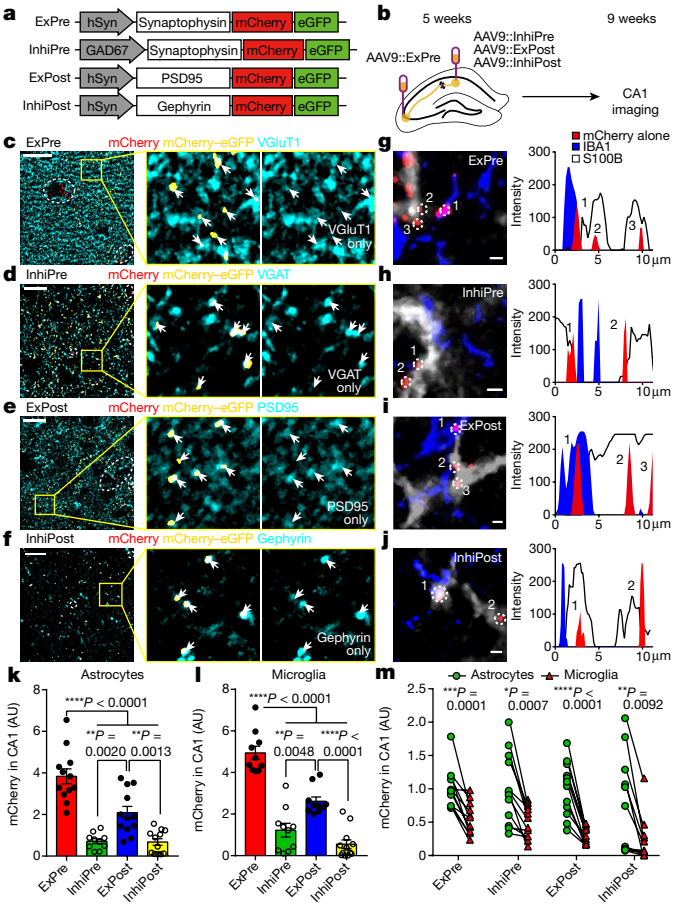

Fig. 1 | Astrocytes dominantly eliminate CA1 synapses in the normal adult hippocampus. a, Schematic illustration of glial synapse elimination reporters. **b**, Experimental scheme of AAV reporter injection. **c**–**f**, Co-localization assays comparing synaptic proteins (cyan) with AAV reporters (yellow for mCherry–eGFP, red in dotted circle for mCherry alone). Left, representative single-plane images; middle and right, expanded views. White arrows indicate co-localization of synaptic proteins and complemented AAV reporters. Scale bars, 10 µm. **g**–**j**, Co-localization assays comparing mCherry-alone puncta (red) with astrocytes (S100B, white) and microglia (IBA1, blue). Left, representative single-plane images; right, fluorescence trajectories of S100B, IBA1 and mCherry-alone puncta. Numbers (1–3) indicate mCherry-alone puncta co-localized with either astrocytes or microglia. **k**–**m**, Quantification comparing the areas of engulfed synapses between reporters (in astrocytes (**k**) and microglia (**l**)) and between astrocytes and microglia (**m**). $n = 12, 10, 12, 12$ (**k**); $n = 10, 10, 10, 12$ (**l**); $n = 12, 12, 12, 11$ (**m**) (from left to right). **k**, **l**, One-way ANOVA followed by Tukey's multiple comparisons test; **m**, paired *t*-test. Mean ± s.e.m.; *n* value represents independent experiments from three mice per group.

into CA3 or CA1 of adult mice (Fig. 1b), the fusion proteins exclusively co-localized with excitatory or inhibitory synapses in CA1 (Fig. 1c–f, Extended Data Fig. 2a, c, e, g). In agreement with our data with the lyn–mCherry–eGFP reporter, many distinct mCherry-alone puncta were found inside glial processes in the CA1 at both excitatory and inhibitory synapses (Fig. 1g–j, Extended Data Fig. 3a, b). Notably, significantly more excitatory synapses than inhibitory synapses were phagocytosed by either astrocytes or microglia (Fig. 1k, l, Extended Data Fig. 4). Furthermore, immunohistochemistry results showed that glial cells contained more VGLUT1$^+$ or PSD95$^+$ excitatory puncta than VGAT$^+$ or gephyrin$^+$ inhibitory synaptic puncta (Extended Data Fig. 5a–d). These data indicate that excitatory synapses in the adult CA1 are the main target of glial phagocytosis. Unexpectedly, we also found more mCherry-alone puncta derived from excitatory or inhibitory synapses in astrocytes than in microglia (Fig. 1m, Extended Data Fig. 5e). This result suggests that, although microglia have been regarded as the major phagocytes in the brain[7–9,12,13], astrocytes participate more actively in eliminating synapses during normal synaptic turnover in the adult CA1.

Detailed analysis of ExPre-derived puncta engulfed by astrocytes showed that 93% of mCherry-alone puncta were localized in lysosomes, whereas only 4.6% of mCherry–eGFP puncta were (Extended Data Fig. 3a, c–e). By contrast, endosomes contained similar percentages of mCherry-alone and mCherry–eGFP puncta, indicating that eGFP lost its signal during its transport from endosomes to lysosomes (Extended Data Fig. 3a, f–h). Some of the mCherry-alone puncta overlapped with synaptic proteins, representing synapse material that was recently engulfed by astrocytes (Extended Data Fig. 2b, d, f, h).

Our findings were not due to any abnormal synaptic properties induced by AAV reporters, because neurons expressing AAV reporters showed normal spontaneous excitatory and inhibitory postsynaptic currents (sEPSCs and sIPSCs, respectively), excitability, and membrane properties (Extended Data Fig. 6e–h, Supplementary Table 1). Furthermore, hippocampal tissue showed no signs of reactive gliosis after reporter injection (Extended Data Fig. 6i–u). Finally, there were no age-dependent changes in astrocytic phagocytosis of excitatory synapses between 3- and 9-month-old hippocampus (Extended Data Fig. 6v–x). Together, these data indicate that our analysis represents endogenous synapse turnover in the adult hippocampus, and that astrocytes contribute to this process by constantly phagocytosing synapses.

Activity-induced synapse elimination

As astrocytic processes associate closely with synapses and respond to their activity[14], we investigated whether astrocytic phagocytosis of synapses was modulated by neuronal activity. To induce hippocampal activity, we exposed mice injected with AAV reporters to environmental enrichment chambers (Fig. 2a) for 2 or 7 days. Both groups of mice showed significant increases in the number of c-FOS-positive cells in CA1 (Extended Data Fig. 7a, b), but only mice that had been exposed to environmental enrichment for 7 days showed enhanced neurogenesis in the dentate gyrus (Extended Data Fig. 7c, d). Unexpectedly, astrocytic uptake of excitatory pre- and post-synapses was significantly increased in both groups of mice (Fig. 2b, Extended Data Fig. 7e). By contrast, neither astrocytic uptake of inhibitory synapses nor microglial uptake of either excitatory or inhibitory synapses (Fig. 2b, c, Extended Data Fig. 7e, f) was affected by neuronal activity elicited by environmental enrichment.

Next, to validate our reporter system with a non-viral method and to examine synapse engulfment from individual synaptic boutons, we expressed ExPre along with fluorescence-tagged hSYN (hSYN–tagBFP) in hippocampal CA3 neurons by electroporation. With this approach, we sparsely labelled excitatory pre-synapses with mCherry–eGFP and filled neuronal processes with tagBFP (Fig. 2d). Similar to our AAV reporter system, many mCherry-alone puncta that originated from individual terminal and en passant boutons (Fig. 2d) were observed inside astrocytic or microglial processes (Fig. 2e, f). In addition, mCherry-alone puncta were found within axons, representing synaptic vesicles that had been recycled by neurons (Extended Data Fig. 7g). Notably, there were significantly more glia-engulfed mCherry-alone puncta and puncta-containing boutons in mice that had experienced 7 days of environmental enrichment than in control mice, whereas there was no difference in recycled mCherry-alone puncta inside axons (Fig. 2g, Extended Data Fig. 7h). Our data suggest that neuronal activity selectively increases phagocytosis of excitatory synapses by astrocytes, and potentially mediates activity-dependent synaptic turnover and plasticity.

MEGF10-dependent synapse phagocytosis

To test whether phagocytosis by astrocytes is involved in synapse engulfment in the adult hippocampus, we generated loxP-floxed

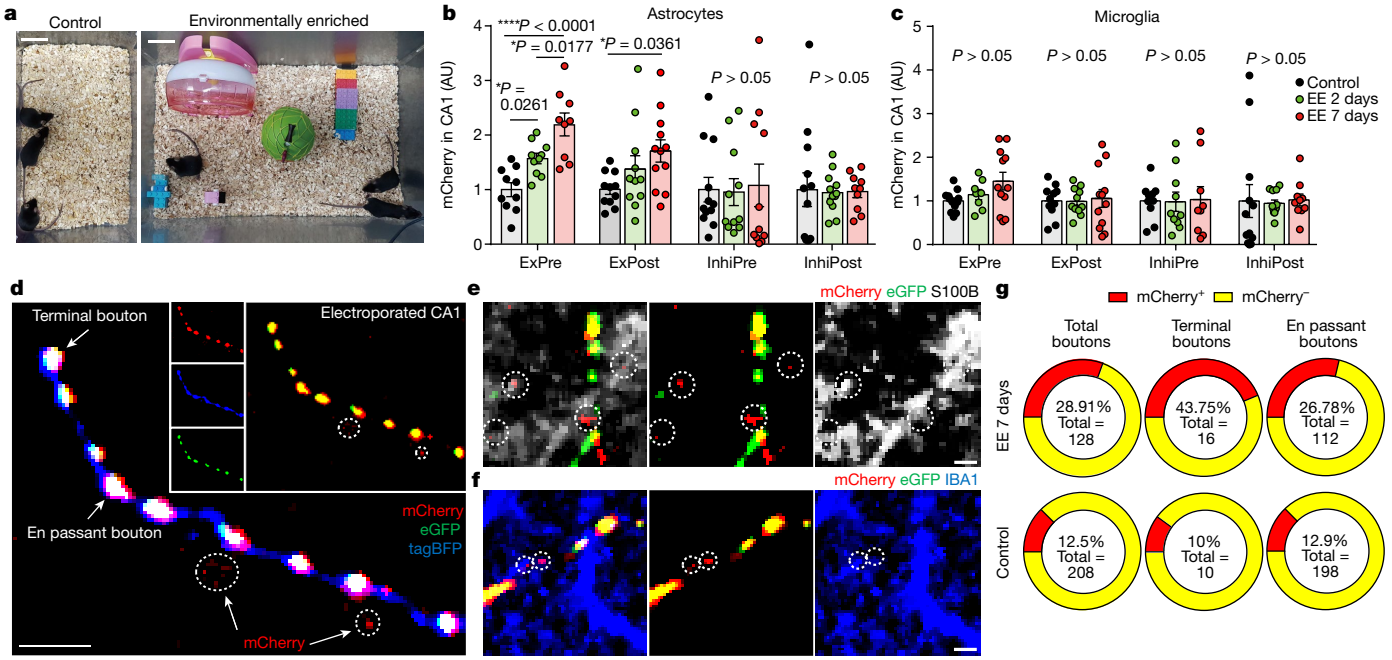

Fig. 2 | Hippocampal activity regulates synapse elimination by astrocytes. **a**, Control (left) and environmentally enriched (right) cages. Scale bars, 5 cm. **b**, **c**, Comparison of the areas of synapses engulfed by astrocytes (**b**) and microglia (**c**) in reporter-injected CA1 from control mice and mice exposed to environmental enrichment (EE) for 2 or 7 days. ExPre (**b**, $n = 9–10$; **c**, $n = 8–12$), ExPost (**b**, $n = 11–12$; **c**, 11–12), InhiPre (**b**, $n = 11–12$; **c**, $n = 9–10$), InhiPost (**b**, $n = 10–12$; **c**, $n = 10–12$). One-way ANOVA followed by Tukey's multiple comparisons test (**b**, **c**). Mean ± s.e.m; n values represent independent experiments from three mice per group. **d**–**f**, Representative z-stack (**d**) or single-plane (**e**, **f**) images of an individual axon labelled with ExPre (yellow) along with h*SYN*–tagBFP (**d**, blue) or glia (**e**, S100B, white; **f**, IBA1, blue). Dotted circles highlight mCherry-alone puncta (red) inside glia. Scale bars, 5 µm (**d**), 1 µm (**e**, **f**). **g**, Percentages of boutons containing mCherry-alone puncta out of all individual boutons. The total number of samples for each group is shown. $n = 5$ mice for each group.

Megf10 (*Megf10*$^{fl/fl}$) mice, in which *Megf10* can be conditionally deleted in a Cre-dependent manner[3]. Inducible deletion of *Megf10* in adult astrocytes was achieved by generating *Aldh1l1-creERT2:Megf10*$^{fl/fl}$ mice and injecting them with 4-hydroxy tamoxifen (4OHT) at 2 months of age for 5 consecutive days (astrocyte-specific conditional *Megf10* knockout: ac*Megf10* KO)[15]. Astrocyte-specific *Megf10* deletion in the hippocampus was verified by immunohistochemistry and western blotting that showed an absence of MEGF10 (Extended Data Fig. 8a, b). In addition, we confirmed that astrocytes in ac*Megf10* KO mice showed no changes in number or areas of territory (Extended Data Fig. 8c–e).

By injecting AAV reporters into ac*Megf10* KO mice, we found that CA1 astrocytes in which *Megf10* had been knocked out showed significantly reduced engulfment of excitatory synapses compared to those in control mice (Fig. 3a, b, e). By contrast, we found no change in astrocytic engulfment of inhibitory synapses (Fig. 3c, d, f), indicating that astrocytes use MEGF10 specifically to eliminate excitatory synapses in the adult hippocampus. Notably, the number of excitatory synapses engulfed by microglia was not affected in ac*Megf10* KO mice, which suggests that microglia do not compensate for the reduced phagocytic function of astrocytes in the adult hippocampus (Extended Data Fig. 8j, k).

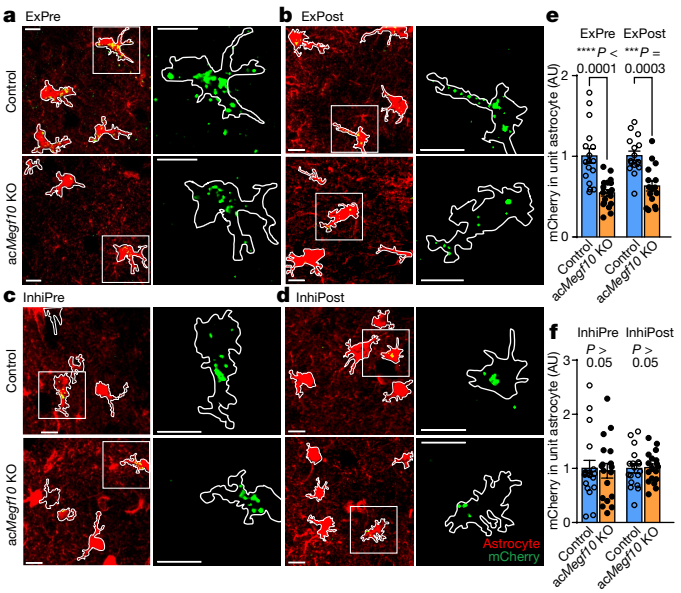

Fig. 3 | Astrocytes eliminate adult hippocampal excitatory synapses via MEGF10. **a**–**d**, Representative z-stack images (left) and expanded panels (right) of astrocytes (S100B, red) with mCherry-alone puncta (green) derived from ExPre (**a**), ExPost (**b**), InhiPre (**c**) or InhiPost (**d**) reporters in CA1 of control and ac*Megf10* KO mice. White outlines show astrocytes. Scale bars, 10 µm. **e**, **f**, Quantification of the areas of synapses engulfed by astrocytes in CA1 of control and ac*Megf10* KO mice injected with ExPre (**e**, $n = 17$ and 18), ExPost (**f**, $n = 16$ and 16), InhiPre (**f**, $n = 18$ and 18) or InhiPost (**f**, $n = 18$ and 18) AAV reporters. Mann–Whitney test (**e**, **f**). Mean ± s.e.m; n values represent independent experiments from four mice per group.

Roles of MEGF10 in circuit homeostasis

To investigate whether astrocytes use MEGF10 for phagocytosis to control synapse numbers in the adult hippocampus, we counted the number of excitatory (Fig. 4b, d) and inhibitory synapses (Fig. 4c, e) in ac*Megf10* KO mice after injection of 4OHT (Fig. 4a). Notably, even with acute deletion of *Megf10* (1 week after the last 4OHT injection), the number of VGLUT1$^+$ excitatory pre-synapses was significantly higher in ac*Megf10* KO mice than in control mice (Fig. 4b, d, Extended Data Fig. 8f–i). Furthermore, the number of either excitatory post-synapses (PSD95$^+$) or

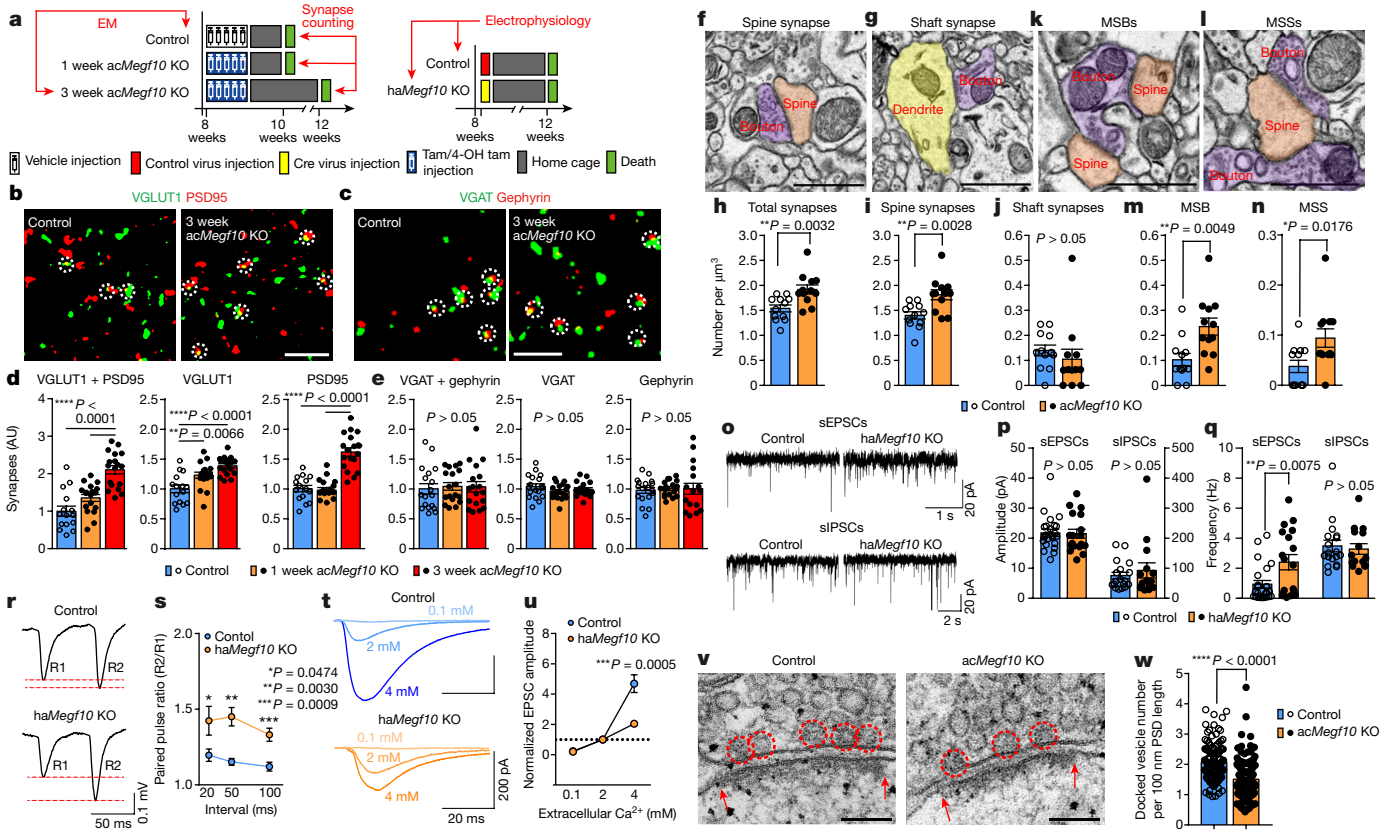

Fig. 4 | Astrocyte MEGF10 maintains the number and function of adult CA1 synapses. a, Experimental schedules of AAV reporter injection and analysis. **b**–**e**, Representative single-plane images (**b**, **c**) and quantification (**d**, **e**) of excitatory (**b**, **d**) and inhibitory (**c**, **e**) synapses in CA1 from control mice ($n = 15$) and ac*Megf*10 KO mice after 1 week or 3 weeks of knockout ($n = 18$ for each group). Dotted circles highlight co-localized synapses. Scale bars, 3 µm. n values represent independent experiments from three mice per group. **f**, **g**, **k**, **l**, Representative ssTEM images of spine (**f**) and shaft (**g**) synapses, MSBs (**k**) and MSSs (**l**). Scale bars, 1 µm. **h**–**j**, **m**, **n**, Numbers of total (**h**), spine (**i**) and shaft (**j**) synapses, MSBs (**m**) and MSSs (**n**). $n = 12$ from three mice per group. **o**–**q**, Representative traces (**o**), amplitudes (**p**) and frequencies (**q**) of sEPSCs (control, $n = 24$; ha*Megf*10 KO, $n = 18$) and sIPSCs (control, $n = 18$; ha*Megf*10 KO, $n = 15$). **r**, **s**, Representative fEPSP traces (**r**) and PPRs (**s**) of control ($n = 10$) or ha*Megf*10 KO mice ($n = 11$) after two consecutive stimuli. **t**, **u**, Representative traces (**t**) and amplitudes (**u**) of evoked EPSCs from control ($n = 7$) and ha*Megf*10 KO slices ($n = 8$) in artificial cerebrospinal fluid (ACSF) with different Ca^{2+} concentrations. n values represent recorded cells (**p**, **q**, **u**) or slices (**s**) from 3–5 mice per group. **v**, **w**, Representative TEM images (**v**) and numbers (**w**) of docked vesicles (in red circles) in control ($n = 135$) and ac*Megf*10 KO CA1 ($n = 154$ axon terminals, 2 mice). Red arrows show postsynaptic density (PSD). Scale bars, 100 nm. **d**, **e**, One-way ANOVA followed by Tukey's multiple comparisons test; **h**–**j**, **m**, **n**, **p**, **q**, **s**, **u**, **w**, unpaired Student's t-test. Mean ± s.e.m.

excitatory synaptic contacts ($VGluT1^+PSD95^+$) was also significantly increased 3 weeks after the last 4OHT injection (Fig. 4d). However, the number of $VGAT^+$ and $gephyrin^+$ inhibitory synapses was not affected by *Megf10* KO in astrocytes (Fig. 4c, e), emphasizing the role of MEGF10 in eliminating excitatory synapses in the adult hippocampus.

When we injected a low titre of AAV5 encoding *Gfap* promoter-driven eGFP–2a–Cre into the $Megf10^{fl/fl}$ CA1, to elicit a mosaic pattern of *Megf10* KO in astrocytes (Extended Data Fig. 8l, m), the number of excitatory synapses was significantly increased only in the territories of *Megf10*-deleted astrocytes (Extended Data Fig. 8n–p), but not in the neighbouring territories of intact astrocytes. These data suggest that MEGF10 acts within a short range, where astrocytic processes can touch and eliminate nearby synapses.

Next, we used 3D reconstruction of scanning electron microscope (SEM) images[16] to identify points at which astrocytes were phagocytosing portions of pre-synapses in CA1 (Extended Data Fig. 9a–f). Consistent with immunohistochemistry data, serial section transmission electron microscopy (ssTEM)[16] results also showed that ac*Megf10* KO mice had significantly more total synapses and spine (excitatory) synapses than control mice, whereas there was no difference in the number of dendritic shaft (inhibitory) synapses (Fig. 4f–j, Extended Data Fig. 9g, h). When we classified spine synapses into multiple synaptic bouton (MSB, a single bouton with multiple spines) or multiple synaptic spine (MSS, a single spine with multiple boutons), both MSBs and MSSs were significantly increased (Fig. 4k–n) in ac*Megf10* KO mice compared to control mice, suggesting that phagocytosis of synapses by astrocytes is required for eliminating redundant synaptic connections in maintaining circuit homeostasis.

Complement-dependent phagocytosis by microglia is involved in hippocampal memory forgetting and engram dissociation in adult mice[12]. To evaluate whether microglia also help to control the number of excitatory synapses in adult CA1, we depleted microglia by feeding mice with PLX3397 chow, which has been shown to kill microglia efficiently[17] (Extended Data Fig. 8q, r). Consistent with previous results[18], depletion of microglia for a month did not alter the number of excitatory synapses in adult mouse brains (Extended Data Fig. 8s).

Next, to evaluate changes in basal synaptic transmission induced by lack of MEGF10 in astrocytes, we analysed sEPSCs or sIPSCs in CA1 pyramidal neurons from $Megf10^{fl/fl}$ mice injected with AAV5 encoding *Gfap* promoter-driven eGFP–2a–Cre or eGFP into CA1 (hippocampus-specific astrocyte conditional *Megf10* knockout: ha*Megf10* KO; Fig. 4a). Although the overall membrane properties of CA1 neurons were unaffected (Supplementary Table 1), the average sEPSC frequency was more than doubled in slices from ha*Megf10* KO mice compared to control mice. However, both frequencies and amplitudes of sIPSCs were unchanged (Fig. 4o–q). There was a

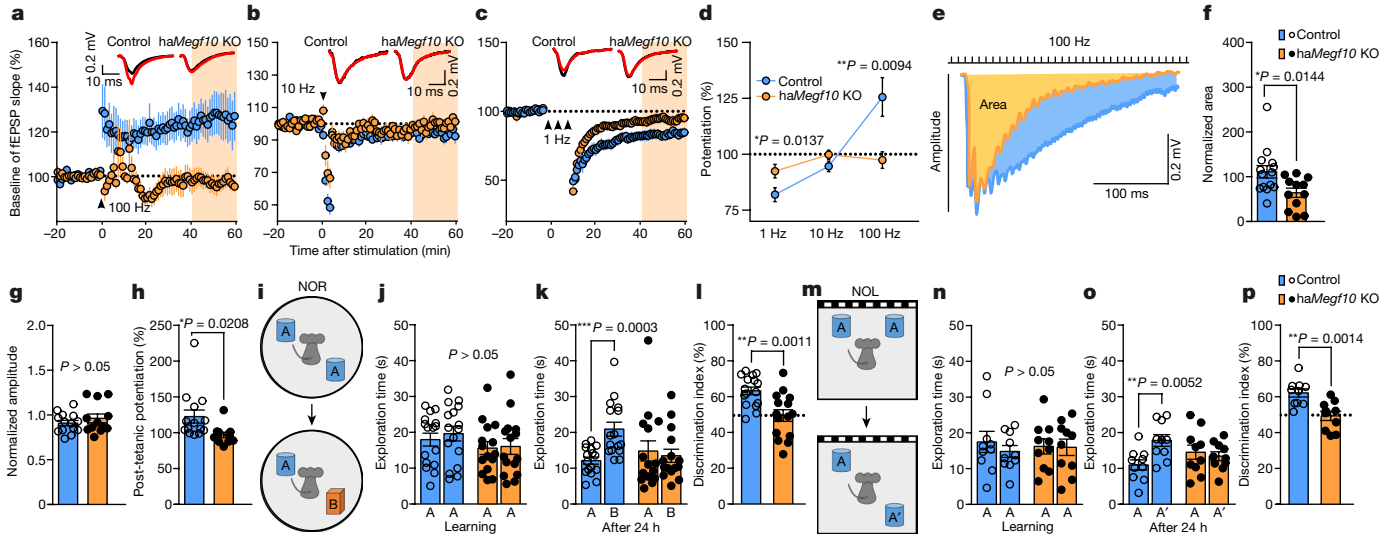

Fig. 5 | Astrocyte MEGF10 mediates synaptic plasticity and memory formation. **a**–**c**, Changes in the strength of Schaffer collateral synapses induced by 100 Hz (**a**), 10 Hz (**b**) or 1 Hz (**c**) frequencies at the indicated time points (black arrowheads). **a**, **b**, 100 stimuli; **c**, 300 × 3 stimuli. Insets, representative fEPSP responses during baseline (black) or 40–60 min after stimuli (red). **a**, Control, $n = 14$ slices from 5 mice; ha*Megf10* KO, $n = 12$ slices from 4 mice. **b**, Control, $n = 8$ slices from 3 mice; ha*Megf10* KO, $n = 8$ slices from 3 mice. **c**, Control, $n = 22$ slices from 4 mice; ha*Megf10* KO, $n = 23$ slices from 3 mice. **d**, Frequency-dependent changes in synaptic strengths. **e**, Representative cumulative fEPSPs during 100-Hz induction of LTP. **f**, **g**, Areas (**f**) and peaks (**g**) of cumulative fEPSPs normalized by baseline. **h**, Post-tetanic potentiation 5 min after stimulation. **i**, Experimental design of NOR test. **j**–**l**, Exploration time during learning (**j**), exploration time during 24-h retrieval tests (**k**), and NOR discrimination index (**l**) for control ($n = 16$) and ha*Megf10* KO mice ($n = 15$). **m**, Experimental design of NOL test. **n**–**p**, Exploration time during learning (**n**), exploration time during 24-h retrieval test (**o**), and NOL discrimination index (**p**) for control and ha*Megf10* KO mice ($n = 10$ for each group). Unpaired Student's *t*-test; mean ± s.e.m.

similar increase in miniature EPSC (mEPSC) frequencies in ha*Megf10* KO slices, but amplitudes of sEPSCs and mESPCs were not affected (Extended Data Fig. 10a–c). These normal amplitudes of sEPSCs and mEPSCs, along with the normal AMPA/NMDA (α-amino-3-hydroxy-5-methyl-4-isoxazolepropionic acid/*N*-methyl-D-aspartate) receptor ratio (Extended Data Fig. 10d, e), indicate that excitatory postsynaptic functions are not altered by astrocytic phagocytosis. We found no significant changes in the evoked EPSC/IPSC ratio of CA1 neurons (Extended Data Fig. 10f-h), indicating that ha*Megf10* KO slices have a normal excitatory/inhibitory ratio.

An increase in the sEPSC or mEPSC frequency can be caused by either an increase in presynaptic release or excessive synaptic connectivity. Our recordings of field excitatory postsynaptic potentials (fEPSPs) showed that the paired pulse ratio (PPR) in ha*Megf10* KO slices was significantly increased (Fig. 4r, s), implying reduced presynaptic release of neurotransmitter. In addition, treatment of ha*Megf10* KO slices with high-Ca^{2+} bath solution did not facilitate Ca^{2+}-dependent vesicular release[19] (Fig. 4t, u). Furthermore, although ac*Megf10* KO had an increase in total vesicle numbers at axon terminals, compared with control mice (Extended Data Fig. 10i, j), the number of docked vesicles located near presynaptic terminals was reduced (Fig. 4v, w). The estimated size of the readily releasable pool (RRP) of neurotransmitter vesicles[20,21] was also significantly smaller in ha*Megf10* KO slices than in control slices (Extended Data Fig. 10k–o).

Together, these results show that normal excitatory synaptic connectivity requires constant regulation by MEGF10-dependent astrocytic phagocytosis. Our data also suggest that defective phagocytosis of synapses by astrocytes triggers homeostatic downregulation of presynaptic release to compensate for the presence of excess synapses and increased excitatory network activity.

Roles of MEGF10 in plasticity and memory

As proper synaptic connection is a prerequisite for synaptic plasticity[22,23], we next tested whether hippocampal long-term potentiation (LTP) or depression (LTD) was affected by deletion of *Megf10*. Complementing our findings in the ac*Megf10* KO mouse brain (Fig. 4), CA1 in ha*Megf10* KO slices showed enhanced basal synaptic transmission in response to strong stimulation (≥150 μA), but not weak stimulation (≤100 μA) (Extended Data Fig. 10p). To examine synaptic plasticity, we stimulated Schaffer collateral fibres in hippocampal slices with various frequencies and compared the resulting changes in fEPSP responses. Unexpectedly, both LTP triggered by 100-Hz and LTD triggered by 1-Hz stimulation were significantly diminished in ha*Megf10* KO slices compared to control slices (Fig. 5a–d). Although the initial fEPSP sizes were similar, accumulation of fEPSPs in response to 100-Hz stimulation was reduced in ha*Megf10* KO slices (Fig. 5e–g). In addition, post-tetanic potentiation immediately after delivery of 100-Hz stimulation was not detected in ha*Megf10* KO slices (Fig. 5h). These results suggest that failure to induce either LTP or LTD is due to abnormal synaptic plasticity caused by excessive but functionally impaired glutamatergic synapses in *Megf10* KO mice.

Next, to test whether astrocytic synapse elimination is involved in memory formation, we challenged the mice with novel object recognition (NOR) and novel object location (NOL) tests[24] (Fig. 5i, m). Control and ha*Megf10* KO mice showed comparable locomotion and spatial navigation activity, as well as normal anxiety levels (Fig. 5j, n, Extended Data Fig. 10q–z). However, ha*Megf10* KO mice displayed a significant deficit in 24-h NOR and NOL memory (Fig. 5k, l, o, p). These data show that astrocytic phagocytosis of adult hippocampal excitatory synapses has a crucial role in regulating learning and memory.

Hippocampal memory traces are thought to be stored transiently and to disappear after several weeks[25]. Moreover, connectivity patterns in the adult CA1 undergo nearly full erasure in about 3–6 weeks[2], which suggests that there must be a mechanism to control such rapid synaptic turnover and re-patterning of connectivity. As we found that astrocytes, but not microglia, constantly eliminate excess synaptic connections, astrocytic phagocytosis may contribute to the rapid renewal of synaptic memory traces in the adult hippocampus.

Our findings have important implications and raise interesting questions—for example, how MEGF10 eliminates unnecessary excitatory synapses, but not inhibitory ones, in response to neuronal activity; and whether the capacity of astrocytic phagocytosis changes during ageing or in neurological diseases. Brains with excessive synaptic connectivity can show disrupted synaptic plasticity and cognitive functions[26,27]. Therefore, it is possible that restoring the constant refinement of synaptic connectivity by modulating MEGF10 may be a novel strategy for the treatment of brain disorders that involve synaptopathologies.

Online content

Any methods, additional references, Nature Research reporting summaries, source data, extended data, supplementary information, acknowledgements, peer review information; details of author contributions and competing interests; and statements of data and code availability are available at https://doi.org/10.1038/s41586-020-03060-3.

1. Toni, N., Buchs, P. A., Nikonenko, I., Bron, C. R. & Muller, D. LTP promotes formation of multiple spine synapses between a single axon terminal and a dendrite. *Nature* **402**, 421–425 (1999).
2. Attardo, A., Fitzgerald, J. E. & Schnitzer, M. J. Impermanence of dendritic spines in live adult CA1 hippocampus. *Nature* **523**, 592–596 (2015).
3. Chung, W. S. et al. Astrocytes mediate synapse elimination through MEGF10 and MERTK pathways. *Nature* **504**, 394–400 (2013).
4. Maletic-Savatic, M., Malinow, R. & Svoboda, K. Rapid dendritic morphogenesis in CA1 hippocampal dendrites induced by synaptic activity. *Science* **283**, 1923–1927 (1999).
5. Okabe, S., Kim, H. D., Miwa, A., Kuriu, T. & Okado, H. Continual remodeling of postsynaptic density and its regulation by synaptic activity. *Nat. Neurosci.* **2**, 804–811 (1999).
6. Xu, T. et al. Rapid formation and selective stabilization of synapses for enduring motor memories. *Nature* **462**, 915–919 (2009).
7. Stevens, B. et al. The classical complement cascade mediates CNS synapse elimination. *Cell* **131**, 1164–1178 (2007).
8. Schafer, D. P. et al. Microglia sculpt postnatal neural circuits in an activity and complement-dependent manner. *Neuron* **74**, 691–705 (2012).
9. Paolicelli, R. C. et al. Synaptic pruning by microglia is necessary for normal brain development. *Science* **333**, 1456–1458 (2011).
10. Leeman, D. S. et al. Lysosome activation clears aggregates and enhances quiescent neural stem cell activation during aging. *Science* **359**, 1277–1283 (2018).
11. Doherty, G. P., Bailey, K. & Lewis, P. J. Stage-specific fluorescence intensity of GFP and mCherry during sporulation in *Bacillus subtilis*. *BMC Res. Notes* **3**, 303 (2010).
12. Wang, C. et al. Microglia mediate forgetting via complement-dependent synaptic elimination. *Science* **367**, 688–694 (2020).
13. Hong, S. et al. Complement and microglia mediate early synapse loss in Alzheimer mouse models. *Science* **352**, 712–716 (2016).
14. Steward, O., Torre, E. R., Tomasulo, R. & Lothman, E. Neuronal activity up-regulates astroglial gene expression. *Proc. Natl Acad. Sci. USA* **88**, 6819–6823 (1991).
15. Srinivasan, R. et al. New transgenic mouse lines for selectively targeting astrocytes and studying calcium signals in astrocyte processes in situ and in vivo. *Neuron* **92**, 1181–1195 (2016).
16. Howard, C. V. & Reed, M. G. *Unbiased Stereology: Three-Dimensional Measurement in Microscopy* 1st edition, 69–105 (Springer, 1999)
17. Elmore, M. R. et al. Colony-stimulating factor 1 receptor signaling is necessary for microglia viability, unmasking a microglia progenitor cell in the adult brain. *Neuron* **82**, 380–397 (2014).
18. Rice, R. A. et al. Elimination of microglia improves functional outcomes following extensive neuronal loss in the hippocampus. *J. Neurosci.* **35**, 9977–9989 (2015).
19. Rhee, J.-S. et al. Augmenting neurotransmitter release by enhancing the apparent Ca^{2+} affinity of synaptotagmin 1. *Proc. Natl Acad. Sci. USA* **102**, 18664–18669 (2005).
20. Schneggenburger, R., Meyer, A. C. & Neher, E. Released fraction and total size of a pool of immediately available transmitter quanta at a calyx synapse. *Neuron* **23**, 399–409 (1999).
21. Elmqvist, D. & Quastel, D. M. J. A quantitative study of end-plate potentials in isolated human muscle. *J. Physiol. (Lond.)* **178**, 505–529 (1965).
22. Caroni, P., Donato, F. & Muller, D. Structural plasticity upon learning: regulation and functions. *Nat. Rev. Neurosci.* **13**, 478–490 (2012).
23. Kandel, E. R. The molecular biology of memory storage: a dialogue between genes and synapses. *Science* **294**, 1030–1038 (2001).
24. Vogel-Ciernia, A. & Wood, M. A. Examining object location and object recognition memory in mice. *Curr. Protoc. Neurosci.* **69**, 1–17 (2014).
25. Tonegawa, S., Morrissey, M. D. & Kitamura, T. The role of engram cells in the systems consolidation of memory. *Nat. Rev. Neurosci.* **19**, 485–498 (2018).
26. Skelton, P. D., Frazel, P. W., Lee, D., Suh, H. & Luikart, B. W. Pten loss results in inappropriate excitatory connectivity. *Mol. Psychiatry* **24**, 1627–1640 (2019).
27. Guang, S. et al. Synaptopathology involved in autism spectrum disorder. *Front. Cell. Neurosci.* **12**, 470 (2018).

Methods

Mice

All mouse experiments were performed according to articles approved by Institutional Animal Care and Use Committee (IACUC) protocols from the Korea Advanced Institute of Science and Technology (KAIST) and the Korea Brain Research Institute (KBRI). We followed all proper ethical regulations. LoxP-floxed *Megf10* (*Megf10*$^{fl/fl}$) mice were generated by Stanford Transgenic, Knockout and Tumour Model Center (TKTC). B6;FVB-Tg(*Aldh1l1-cre/ERT2*)1Khakh/J (*Aldh1l1-creERT2*) mice were obtained from Jackson laboratories (JAX). For measuring the phagocytic ability of astrocytes and the number of synapses in *Megf10*-deleted mice, as well as for ssTEM experiments, *Megf10*$^{fl/fl}$ and *Aldh1l1-creERT2* lines were crossed together to produce *Aldh1l1-creERT2:Megf10*$^{fl/fl}$ (ac*Megf10* KO) mice. *Megf10*$^{tm1(KOMP)Vlcg}$ (straight *Megf10* knockout) mice[3] were obtained from the Barres laboratory. All mouse lines were maintained by breeding with C57BL/6 mice in standard plastic cage (29 cm × 17.5 cm × 18 cm). All experiments that involve mutant mice were performed blindly with other littermates. All mice were randomly assigned to experiments. For imaging, electrophysiology and EM experiments, *Mus musculus* (C57BL/6) were used. Genders were not considered. The mice were killed at the age of 9 weeks to 12 weeks. For behaviour experiments, all mice used were the C57BL/6J background strains of either sex at 8–14 weeks old. *Megf10*$^{fl/fl}$ mice were used for slice electrophysiology and behavioural experiments. For experimental purposes, wild-type C57BL/6 mice were purchased from Daehan BioLink (DBL) and Samtaco. No statistical methods were used to predetermine sample size.

Generation of *Megf10*-flox mice

Megf10-flox mice were generated using a construct generated by the trans-NIH Knockout Mouse Project (KOMP) and obtained from the KOMP Repository (https://www.komp.org). C57BL/6 embryonic stem (ES) cells were used for electroporating the *Megf10* conditional KO construct and correctly targeted ES cells were screened by Southern blot. The resulting chimeric males were bred with C57BL/6 wild-type females to obtain *Megf10*-flox founder mice. All experiments were performed with the support from the Stanford TKTC.

AAV production

To produce AAVs, we co-transfected a pAAV9 capsid plasmid, a virus assembly helper plasmid (pAd deltaF6, UPENN vector core), and target plasmids into HEK293T (Korean Cell Line Bank) cells using the PEI (1 mg/ml)-based transfection method[28]. pAAV ::hSyn-Synaptophysin-mCherry-eGFP (ExPre), pAAV::GAD67-synaptophysin-mCherry-eGFP (InhiPre), pAAV::hSyn-lyn-mCherry-eGFP, pAAV-CW3SL::hSyn-PSD95-mCherry-eGFP (ExPre) and pAAV-CW3SL::hSyn-gephyrin-mCherry-eGFP (InhiPost) were packaged with AAV9. HEK293T cells were maintained with fetal bovine serum (FBS, Gibco)-containing Dulbecco's modified Eagle's medium (DMEM, Gibco), which was replaced with serum-free medium during transfection (6–18 h). Transfected cells were incubated in a 37 °C, 5% CO_2 conditioned cell incubator for 72 h. Collected cells were resuspended with 50% fresh DMEM, 0.04% DNase I (Worthington) in nuclease-free water, then lysed with a series of freeze and thaw cycles. AAV-containing supernatant was obtained and AAVs were further purified using the polyethylene glycol (PEG)-mediated purification method[29]. Purified AAVs were concentrated using a 50-kDa Amicon ultra centrifugal filter tube (Millipore) to 200 µl. The titre of AAVs was measured using an AAVpro titration kit (Takara, version 2).

AAV stereotaxic injection

Mice (4–8 weeks old) were anaesthetized with 1 ml isoflurane (Piramal) in a sealed plastic box; the anaesthetized state was maintained using a veterinary vaporizer (Surgivet). Either AAV9::hSyn-lyn-mCherry-eGFP (5.6×10^{11} genome copies per ml, GC/ml) or AAV9::ExPre (5.3×10^{11} GC/ml) was stereotaxically injected unilaterally into the left lateral geniculate nucleus (LGN; ML: 2.0 mm, AP: −2.1 mm from bregma, DV: −2.55 mm from brain surface) or CA3 (ML: 2.35 mm, AP: −2.0 mm from bregma, DV: −2.25 mm from brain surface) of 4-week-old mutant and control mice. Either AAV9::InhiPre (8.8×10^{11} GC/ml), AAV9::ExPost (4.5×10^{11} GC/ml) or AAV9::InhiPost (9.23×10^{10} GC/ml) was stereotaxically injected unilaterally into the left CA1 (ML: 1.4 mm, AP: −2.0 mm from bregma, DV: −1.45 mm from brain surface) of 4-week-old mutant and wild-type mice. Either AAV5::GFAP (0.7)-Cre-eGFP-T2A-iCre-WRPE (6.4×10^{12} GC/ml) or AAV5::GFAP (0.7)-eGFP-WPRE (1.2×10^{13} GC/ml, Vector Biolabs) was stereotaxically injected bilaterally into CA1 (ML: ±2.0 mm, AP: −1.9 mm from bregma, DV: −1.4 mm from brain surface). All surgery was performed with a stereotaxic frame (Kopf) and either a motorized Hamilton syringe pump (Harvard apparatus) or Nanojector III (Drummond). Pre-pulled glass pipettes were used as an injection needle (WPI), and glass pipette pulling was done using a motorized pipette puller (Sutter Instruments). After injection, the incision on the head was closed with silk suture (Woori Medical). After surgery, mice recovered in a heated cage for an hour before being returned to their home cage.

Molecular cloning and plasmid preparation

pAAV::hSyn-lyn-mCherry-eGFP. We purchased the lyn-tailed (lyn) mCherry-SEpHluorin (Addgene32002) vector. The vector was digested with BamH1 and Not1 (New England Biolab) for an hour at 37 °C to exclude the SEpHluorin gene. Then, BamH1 and Not1-flanked eGFP (produced by PCR) was inserted into the digested vector to produce the lyn-mCherry-eGFP plasmid. Next, we inserted Kpn1 and Hind3 restriction sites into the 5′ and 3′ ends of lyn-mCherry-eGFP by PCR. After gel extraction (Bionics), the Kpn1- and Hind3-flanked lyn-mCherry-eGFP (digested by complementary enzymes, New England Biolab) was inserted into an equivalently digested AAV backbone vector with the h*SYN* promoter.

pAAV::hSyn-Synaptophysin-mCherry-eGFP (ExPre). We purchased the Syn-ATP (synaptophysin-mCherry-luciferase, Addgene item no. 51819) vector. We amplified the gene encoding synaptophysin-mCherry with the two primers for Gibson assembly[30] (annealing sites capitalized) by PCR: 5′-cgcagtcgagaaggtaccATGGGCGAGCTGGATCGCAT-3′ and 5′-ctcaccatggtggcggaTCCCTTGTACAGCTCGTCCATGCCG-3′. After gel extraction, the amplified insert and digested vector (pAAV::hSyn-lyn-mCherry-eGFP digested with Kpn1 and BamH1, New England Biolab) were assembled by Gibson assembly reaction (New England Biolab).

pAAV::GAD67-synaptophysin-mCherry-eGFP (InhiPre). The pGreenZeo-GAD67-Differentiation reporter (SBI, SR10023Pa-1) was obtained from Hyung-ju Park's laboratory (KBRI). We inserted Xba1 and Kpn1 restriction sites into the 5′ and 3′ ends of the *Gad67* promoter in the donated vector by PCR. The vector (pAAV::hSyn-synaptophysin-mCherry-eGFP) was digested with Xba1 and Kpn1 (New England Biolab) to exclude the h*SYN* promoter sequence. The digested *Gad67* promoter fragment was inserted into the digested pA AV::hSyn-Synaptophysin-mCherry-eGFP (without h*SYN*) by ligation.

pAAV-CW3SL::hSyn-PSD95-mCherry-eGFP (ExPost). We synthesized BstAP1-hSyn-PSD95-mCherry-eGFP-XhoI (restriction sites underlined) using the Genscript gene synthesis service (Genscript). Owing to the relatively large size of hSyn-PSD95-mcherry-eGFP with WRPE and hGHpA (5,262 bp) for conventional AAV packaging, we decided to insert our gene into pAAV-CW3SL, an AAV vector that can harbour larger inserts (0.8 kb more) because of the shortened and optimized WRPE and hGHpA sequences[31]. We purchased the pAAV-CW3SL-EGFP plasmid (Addgene item no. 61463) and digested it with BstAP1 and Xho1 (New England Biolab). This reaction excluded eGFP from the

pAAV-CW3SL-eGFP. The synthesized gene was equivalently digested and inserted into the digested vector.

pAAV-CW3SL::hSyn-gephyrin-mCherry-eGFP (InhiPost). We purchased the pCMV-mCherry-gephyrin plasmid (or pmCherry C2-Gephyrin P1, Addgene item no. 68820). We inserted Kpn1 and EcoR1 restriction sites into the 5′ and 3′ ends of the gephyrin open reading frame (ORF) by PCR. The vector (pAAV-CW3SL::hSyn-PSD 95-mCherry-eGFP) was digested with Kpn1 and EcoR1 (New England Biolab) to exclude the PSD95 ORF sequence. The digested gephyrin ORF fragment was inserted into the digested pAAV-CW3SL ::hSyn-Gephyrin-mCherry-eGFP (without the PSD95 ORF) by ligation.

hSyn-tagBFP. The plasmid hSyn−tagBFP was generously donated from the Ben Barres group. All cloned plasmids were transformed into Stbl3 (Invitrogen). Candidate plasmids were prepared from inoculated broth by mini prep and sent for Sanger sequencing service (Bioneer) for validation.

Immunohistochemistry

Mice were anaesthetized with avertin (20 µl/g) by intraperitoneal injection. Anaesthetized mice were perfused with 1× PBS (Welgene) followed by 4% paraformaldehyde in 1× PBS (Wako Chemicals). Brains were isolated, and then post-fixed overnight in fixative at 4 °C. Brains were transferred to 30% sucrose in 1× PBS for 72 h, and then embedded in OCT compound (Leica). Forty-micrometre brain sections were prepared on cryo-stat microtomes (Leica). Appropriate sections were collected and embedded in blocking buffer (4% bovine serum albumin, 0.3% Triton X-100 in 1× PBS) for 1 h at room temperature (RT). Then, appropriate primary antibodies diluted in blocking buffer were added to brain sections for 24 h at 4 °C. The primary antibodies used were as follows: rabbit anti-S100b (Abcam), rabbit anti-IBA1 (Wako), chicken anti-GFAP (Sigma), goat anti-cathepsin D (R&D Systems), guinea pig anti-VGAT (Synaptic Systems), guinea pig anti-VGLUT1 (Millipore), rabbit anti-c-Fos (Cell Signaling), rabbit anti-DCX (Doublecortin, Abcam), mouse anti-NeuN (Millipore), rabbit anti-MEGF10 (Millipore), rabbit anti-PSD95 (Invitrogen), rabbit anti-gephyrin (Synaptic Systems), chicken anti-GFP (Aves Labs), goat anti-IBA1 (Novus), rat anti-RFP (for mCherry, Chromotek), rat anti-mCherry (Invitrogen) rabbit anti-DsRED (Clontech), rabbit anti-tRFP (for tagBFP, Evrogen), rabbit anti-RAB5 (Abcam), guinea pig anti-S100B (Synaptic systems), and rat anti-CD68 (Bio-Rad).

After the brain sections had been washed with PBST (0.1% Tween 20 in 1× PBS), they were treated with appropriate secondary antibodies conjugated with Alexa fluorophore (Invitrogen, Abcam) in PBST for 3 h at room temperature. The sections were washed again with PBST, then mounted on adhesive-coated slideglasses (Matsunami or Fisher Scientific). After all sections were fully adhered to slideglasses, TrueBlack (Biotium) diluted to 1/20 in 70% ethanol was applied to the sections for two minutes at RT to eliminate auto-fluorescent signals by lipofuscin. Remaining agent was washed out with PBST, and Vectashield with or without DAPI (Vector Lab) was used as mounting medium. Prepared samples were stored at −20 °C until imaging.

All images were acquired with a Zeiss LSM 880 confocal upright microscope.

In vivo electroporation

Neonatal (P0) pups were anaesthetized by exposing them to hypothermic conditions for 3 min. The plasmid cocktail (pAAV-hSyn-synaptophysin-mCherry-eGFP and pAAV-hSyn-tagBFP, 2 µg/µl, in the same cocktail containing 0.5% trypan blue) was loaded into a prepulled glass pipette. The pipette was then perpendicularly inserted into a point 1/3 of the distance from lambda to the right eye. Two microlitres of cocktail was injected into the right ventricle at a depth of 2 mm under the insertion point. Only mice with clear blue ventricles were collected. Successfully injected mice were given five serial electric pulses (110 V for 50 ms with 950 ms interval) using a NEPA 21 Type II Super electroporator (Nepa gene) and CUY650P5 electrode tweezer (Nepa gene). For targeting DNA into the hippocampus, a negative electrode was placed above the injection site and a positive electrode was placed next to the opposite jaw. Electroporated pups were placed in a pre-warmed paper box until they recovered healthy movement and a pink skin colour, and subsequently returned to their home cages. The pups were raised to 8 to 12 weeks old and killed. Transfected axons were mainly found in the lateral hippocampal CA1.

Environmental enrichment

Mice were co-housed in relatively bigger cages (40 cm × 24 cm × 18 cm) with a running wheel, melon-shaped nesting material and Lego brick toys (elephants, flamingos and bridges). Control group mice were co-housed in standard plastic cages (described above) until the next experimental steps. Mice were moved to the environmental enrichment cage either 48 h (2 days) or 168 h (7 days) before being killed. We killed all mice on a synchronized day (28 days after virus injection).

Glial engulfment quantification

Confocal images from the brain sections were acquired with a Zeiss LSM 880 (63× or 40× oil immersion optical lens) for quantification as described below. In plots, each data point represents confocal optical sections containing at least 10–15 astrocytes or 7–10 microglia in the imaging volume. Three or four different data points were acquired from one mouse.

All channels including the red-coloured (mCherry), green-coloured (eGFP) and infrared-coloured (astrocytes or microglia) were split using Image J software. mCherry-alone puncta were isolated by subtracting eGFP signals from mCherry signals. Any mCherry puncta overlaid with minimum eGFP signal was excluded from further quantification and image processing steps. Individual confocal single-plane images of stacks of isolated mCherry-alone, green and infrared signals were analysed. Colocalization assays were done using the Diana plugin[32].

To prevent complication due to the potentially different expression levels of the AAV synaptic reporters, we converted the images of mCherry-alone puncta into black and white thresholded images. Then, the area of mCherry-alone puncta was measured. This value was further normalized with the area of glial cells (to compensate for potential difference in density of glial cells) and area of mCherry−eGFP-labelled synapses (to compensate for potential difference in AAV injection). So, each value represents the area of mCherry-alone puncta in glia/(the area of mCherry−eGFP puncta × the area of glial cells).

In Fig. 1l, m, where we compared the amount of engulfed synapses among different types of synapses, we introduced an additional normalization value to consider the differences in synaptic reporter puncta size labelled by the ExPre, InhiPre, ExPost and InhiPost reporters. So each value represents the area of mCherry-alone puncta in glia/(the area of mCherry−eGFP puncta × the area of glial cells × the area of mean synaptic reporter puncta).

In Fig. 1n, where we compared the amount of engulfed synapses by total astrocytes with total microglia in the same imaging fields, the area of glial cells and the area of mean synaptic reporter puncta were not considered. So each value represents the area of mCherry-alone puncta in glia/the area of mCherry−eGFP puncta.

Synapse number quantification

Confocal images from brain sections were acquired using a Zeiss LSM 880 (63× oil immersion optical lens) for quantification as described below. Each data point represents confocal optical sections, and 3–6 data points were acquired from one mouse

All channels including presynaptic and postsynaptic compartments were split using Image J software. The co-localization assay

was done using the Diana plugin as described above. The number of presynaptic-only or postsynaptic-only puncta, as well as the number of co-localized puncta (pre- and postsynaptic together), were measured using the Diana plugin.

Confocal analysis

Confocal images from the brain sections were acquired using a Zeiss LSM 880 (63× or 40× oil immersion optical lens) for quantification as described below. Each data point represents confocal optical sections, and 2–4 data points were acquired from one mouse.

To quantify cathepsin D^+ lysosomes in astrocytes or $CD68^+$ vesicles in microglia, the areas of lysosomes or CD68 within glial cells were isolated and measured using the Diana plugin. To compensate for differences in the density of glial cells, the area of lysosomes or CD68 was normalized to the area of astrocytes or microglia, respectively.

To quantify the immunoreactivity of GFAP, the fluorescent intensity of GFAP in an individual optical section was measured.

To quantify c-Fos^+ neurons in the CA1 pyramidal cell layer, NeuN and c-Fos double-positive cells were manually counted and normalized to the area of confocal optical sections.

To quantify doublecortin (DCX)-positive newborn cells in the dentate gyrus, the number of DAPI signals surrounded by DCX was manually counted and normalized to the area of confocal optical sections.

To quantify the engulfed synaptic proteins by astrocytes or microglia, co-localizing fractions between synaptic proteins (for example, VGluT1, PSD95, VGAT and gephyrin) and glial cells (for example, S100B-positive astrocytes or IBA1-positive microglia) were isolated and measured using the Diana plugin. To compensate for differences in the density of glial cells, the areas of these fractions were normalized to the area of astrocytes or microglia, respectively.

Immunoblotting of MEGF10 protein

Before mice were killed, to avoid potential MEGF10 contamination from blood cells (for example, macrophages), mice were perfused with ice-cold PBS. The two hippocampi were dissected out and homogenized in RIPA lysis buffer (Atto) supplemented with protease inhibitor (Roche Diagnostics). The hippocampal homogenate was incubated on ice for 2 h and only soluble fractions were acquired after 15,000-rpm centrifugation for 15 min at 4 °C. Soluble protein fractions were diluted with SDS-containing sample buffer and separated on 4–20% gradient polyacrylamide gel (Bio-rad). Proteins on the gel were blotted onto methanol-activated PVDF membrane and incubated with 10% skimmed milk in TBST (0.1% Tween 20 in TBS) for 1 h at room temperature. Then, rabbit anti-MEGF10 (Millipore) and mouse anti-GAPDH (Santa Cruz) antibodies were diluted in 10% skimmed milk in TBST and added to the blotted membranes overnight at 4 °C on a rocker. After the membranes were washed with TBST, they were treated with appropriate secondary antibodies conjugated with horseradish peroxidase (Santa Cruz) diluted in 3% skimmed milk in TBST for 2 h at room temperature. The membranes were washed again with TBST and exposed to substrate for the ECL reaction. Luminescence-expressing protein bands were developed on a photosensitive film. MEGF10 and GAPDH bands were blotted on the same membrane and developed separately owing to different light exposure conditions.

4OHT and tamoxifen formulation

4OHT (Sigma) was suspended in pure ethanol at a concentration of 40 mg/ml (Millipore). Then suspended 4OHT was diluted 1:1 with Cremophor/Kolliphor (Sigma), and stored at −20 °C. Before usage, dissolved 4OHT was diluted 1:1 with 1× dPBS and then injected intraperitoneally into mice at a dose of 7.5 µl/g.

Tamoxifen (Sigma) was dissolved in pure corn oil (Sigma) at a concentration of 20 mg/ml, and stored at −20 °C. Before usage, dissolved tamoxifen was heated to 55 °C, and then injected intraperitoneally into mice at a dose of 3.75 µl/g. To achieve maximum Cre recombination in target cells, 4OHT or tamoxifen in vehicle was injected into mice for 5 consecutive days (once per day).

Microglia depletion

To deplete microglia in the adult brain, chow was replaced with PLX3397 (Plexxikon) or PLX5622 (MedChemExpress) chow with a final dose of 600 mg/kg or 1,200 mg/kg, respectively. PLX3397 or PLX5622 chow was given to mice between postnatal weeks 8 and 12 to fully deplete microglia in the brain.

Tissue preparation using heavy metal staining protocol

Mice were deeply anaesthetized with sodium-pentobarbital and intracardially perfused with 0.15M cacodylate buffer and then 2% paraformaldehyde and 2.5% glutaraldehyde in 0.15 M cacodylate buffer (pH 7.4). The pre-fixed brain was removed and stored in the same fixative overnight at 4 °C. Brain slices (150 µm thick) were cut on a vibratome (Leica) in ice-cold 0.15 M cacodylate buffer, and small pieces of hippocampal tissue were stored overnight in the same fixative at 4 °C. Hippocampal tissues were dissected and then washed with the same buffer several times. Tissues were post-fixed with 2% osmium tetroxide (OsO_4)/1.5% potassium ferrocyanide (EMS, Sigma) for 1 h on ice and washed several times. Tissues were placed in 1% thiocarbohydrazide (TCH) (Ted Pell) solution for 20 min and then placed in 2% aqueous OsO_4 for 30 min. Thereafter, tissues were incubated in 2% uranyl acetate (EMS) overnight and in lead aspartate solution at for 30 min to enhance membrane contrast. Hippocampal tissues were dehydrated using a graded series of ethanol (20%, 50%, 70%, 90%, and 100%) on ice, and then infiltrated with acetone, a mixture of resin and acetone, and 100% resin. The resin was prepared from the Epon 812 kit (EMS) following the manufacturer's instructions. Samples were placed in embedding tubes with fresh Epon mixture at 60 °C for 2 days.

Analysis of synaptic density and total vesicles using ssTEM

Embedded samples were trimmed, and 60–70-nm serial sections were cut from the block using an ultramicrotome (RMC) with a diamond knife (Diatome), mounted on Formvar/Carbon (EMS)-coated single slot grids. All images were from the middle of the stratum radiatum (SR) about 150–200 µm from the hippocampal CA1 pyramidal cell soma. At each position an area of $15 \times 15\ \mu m^2$ was captured by the photomontage software for Tecnai 20 TEM (FEI) at an accelerating voltage of 120 kV. The serial mosaiced TEM images were aligned using the FIJI software TrakEM2 plug-in. To estimate synapse densities per unit volume, we used the physical dissector technique, which is an efficient and unbiased stereological counting method[16]. For each mouse, 20–30 serial images obtained from the CA1 SR were manually fine-tune aligned and the number of synapses was counted using the dissector frame with Reconstruct software[33]. To count the number of synapses, synapses were classified by presynaptic vesicles and existence of a clear PSD. The number of synapses per unit volume was calculated as described[16]. To analyse the total number of presynaptic vesicles, the axon terminal area and vesicle were manually tracked and counted using Reconstruct software.

Imaging astrocytes for large areas using SEM

Embedded samples were trimmed, and 60-nm serial sections were cut from the block using an ultramicrotome (Leica) with a diamond knife (Diatome) into the knife holder. The indium-tin-oxide (ITO)-coated glass coverslips were cleaned manually with isopropanol and the serial sections were mounted onto ITO-coated coverslips. All images were from the SR about 100–200 µm from the hippocampal CA1 pyramidal cell soma. At each serial position an area of $80 \times 80\ \mu m^2$ was imaged by the ZEISS Atlas5 software for Gemini 300 SEM (ZEISS) at an accelerating voltage of 5 kV. Image resolution in the x–y plane was 5 nm/pixel. A total of 127 SEM images were obtained from the control mouse, and serial SEM images were fine-tune aligned using the FIJI software

TrakEM2 plug-in. As serial images, images that included synapses being engulfed by astrocytes were manually tracked and 3D-reconstructed using Reconstruct software.

Analysis of docked vesicles using using conventional TEM

Tissue preparation was carried out as for the heavy metal staining protocol until pre-fixation. Samples were post-fixed with 2% OsO_4 (EMS) for 1 h at RT and washed several times. Thereafter, tissues were incubated in 2% uranyl acetate (EMS) overnight. Hippocampal tissues were dehydrated using a graded series of ethanol (20%, 50%, 70%, 90%, and 100%) at RT, infiltrated with acetone, a mixture of resin and acetone, and 100% resin. The resin was prepared from the Epon 812 kit (EMS) following the manufacturer's instructions. Samples were placed in embedding tubes with fresh Epon mixture at 60 °C for 2 days. Embedded samples were trimmed, and 60–70 nm sections were cut from the block using an ultramicrotome (Leica) with a diamond knife (Diatome), mounted on Formvar/Carbon (EMS)-coated single slot grids. Ultrathin sections on grids were then stained with UranyLess (EMS) for 2 min and 3% lead citrate (EMS) for 1 min.TEM images were taken at 20,000× magnification on a Tecnai 20 TEM (FEI). All images were from the middle of the SR about 150–200 μm from the hippocampal CA1 pyramidal cell soma. To count the number of docked vesicles, an image with clear PSD and active zone was used, and synaptic vesicles were manually counted from the presynaptic plasma membrane to 50 nm. For quantification, the number of docked vesicles was divided by 100 nm of PSD length[34].

Whole-cell patch clamp

For whole-cell patch clamp recordings, acute brain slices were obtained from 8–14-week-old mice. The standard ACSF consisted of (in mM) 124 NaCl, 2.5 KCl, 1.2 NaH_2PO_4, 24 $NaHCO_3$, 5 HEPES, 2 $CaCl_2$, 2 $MgCl_2$, and 13 glucose (pH 7.3). Mice were deeply anaesthetized with isoflurane and transcardially perfused with ~20 ml of the slicing ACSF containing (in mM) 93 *N*-methyl-D-glutamine (NMDG)-Cl, 93 HCl, 2.5 KCl, 1.2 NaH_2PO_4, 30 $NaHCO_3$, 20 HEPES, 5 sodium ascorbate, 2 thiourea, 3 sodium pyruvate, 12 *N*-acetyl-L-cysteine (NAC), 0.5 $CaCl_2$, 10 $MgCl_2$, and 25 glucose (pH 7.3) before the brain was dissected. Horizontal slices containing the hippocampus (400-μm thick) were prepared using a VF-200-OZ Compresstome (Precisionary) using the slicing ACSF and recovered at 30–32 °C in the recovery ACSF (in mM; 104 NaCl, 2.5 KCl, 1.2 NaH_2PO_4, 24 $NaHCO_3$, 5 HEPES, 5 sodium ascorbate, 2 thiourea, 3 sodium pyruvate, 12 NAC, 2 $CaCl_2$, 2 $MgCl_2$, and 13 glucose; pH 7.3) for 1 h before recording. Slices were placed in a recording chamber, submerged, and continuously perfused (2–3 ml/min) with an oxygenated standard ACSF (20–25 °C). Data were acquired through a Multiclamp 700B amplifier (Molecular Devices), filtered at 5 kHz, digitized at 10–50 kHz, stored on a computer, and analysed offline using pCLAMP 10 software (Axon Instruments). Borosilicate glass patch electrodes with a resistance of 3–5 MΩ after filling with pipette solution containing (in mM) 140 Cs-methanesulfonate, 7 NaCl, 0.2 EGTA, 2 $MgCl_2$, 4 Mg-ATP, 0.3 Na_2-GTP, 10 Na_2-phosphocreatine, and 10 HEPES (pH 7.3, 290–300 mOsm) were used for recording sEPSCs. Also, to record sIPSCs, the pipette solution contained (in mM) 140 CsCl, 7 NaCl, 0.2 EGTA, 2 $MgCl_2$, 4 Mg-ATP, 0.3 Na_2-GTP, 10 Na_2-phosphocreatine, and 10 HEPES (pH 7.3, 290–300 mOsm). Bicuculline (10 μM; Tocris), 2,3-dihydroxy-6-nitro-7-sulfamoyl-benzo quinoxaline-2,3-dione (NBQX, 10 μM; Tocris), and D-2-amino-5-phosphonovaleric acid (D-AP5, 50 μM; Tocris) were added to the standard ACSF to inhibit GABAergic and glutamatergic synaptic transmission, respectively. During recording of mEPSCs, tetrodotoxin (1 μM, Alomone) was added to the standard extracellular solution to block spontaneous action potentials.

To evoke EPSCs or IPSCs in CA1 neurons, a bipolar electrode (CBBPE75; FHC) was placed on the SR in the CA1 area. To identify excitatory/inhibitory balance, evoked EPSCs (eEPSCs) and IPSCs (eIPSCs) were recorded in the same CA1 neuron by using the same pipette solution as was used for other EPSC recordings. Both eEPSCs and eIPSCs were recorded at holding potentials of −70 mV and 0 mV, respectively, to determine the EPSC/IPSC ratio. eEPSC and eIPSCs were validated by application of NBQX + APV and bicuculline, respectively, in independent experiments (data not shown).

The AMPAR- or NMDAR- dependent eEPSC (AMPA/NMDA) ratio was estimated by calculating the AMPAR-mediated eEPSC amplitude (holding potential of −70 mV) divided by the NMDAR-mediated one (holding potential of +40 mV). The amplitude of NMDAR-mediated eEPSC was measured 60–65 ms after applying electrical stimulation.

To estimate the size of the RRP, repetitive electrical stimulation (20 Hz, 100 stimuli) was applied to evoke multiple EPSCs[35]. The size of the RRP was analysed by using pClamp 11.0.3 and calculated using two methods. In the SMN method[20], the cumulative eEPSC responses during a 20-Hz stimulation were plotted against stimulus numbers. A linear line was fitted to the late point of the cumulative eEPSC response in a range of 4–5 s and back-extrapolated to the *y*-axis to estimate the RRP size. Using the EQ method[21], the eEPSC amplitudes during a 20-Hz stimulation were plotted against the cumulative eEPSC response. Plots were linearly fitted from the sixth to the twentieth cumulative eEPSC and linear fits were back-extrapolated to the *x*-axis to estimate the RRP.

Facilitation and depression of eEPSC responses induced by changes in extracellular Ca^{2+} concentration were recorded from CA1 neurons by exchanging normal Ca^{2+} (2 mM) ACSF solutions with high Ca^{2+} (4 mM) or low Ca^{2+} (0.1 mM) solutions. After acquiring at least 10 min of stable eEPSC responses in normal Ca^{2+} bath solution, high or low Ca^{2+} ACSF solution was perfused. Normalized eEPSC amplitudes were calculated by dividing amplitudes of eEPSCs with high or low Ca^{2+} bath solution by those with the normal Ca^{2+}.

To test the excitability of CA1 neurons, whole-cell current clamp recording was performed by using a pipette solution containing (in mM) 140 K-gluconate, 10 HEPES, 7 NaCl, 4 Mg-ATP, 0.3 Na_2-GTP (pH 7.3, 290–300 mOsm). Current were injected from −50 pA to 250 pA (every 50 pA) for 800 ms, and the number of current-evoked action potentials was counted.

All whole-cell patch clamp recording data were analysed using pClamp 11.0.3. mEPSCs were detected with an amplitude threshold of 5 pA, using MiniAnalysis 6.0 software.

Extracellular fEPSP recording

For extracellular fEPSP recordings, acute hippocampal slices were prepared with a modified sucrose-based slicing ACSF (in mM; 5 KCl, 1.25 NaH_2PO_4, 26 $NaHCO_3$, 0.5 $CaCl_2$, 10 $MgCl_2$, 10 D-glucose and 212.5 sucrose). Coronal slices (400 μm thick) from isolated hippocampi were prepared using a VF-200-OZ Compresstome (Precisionary) and ice-cold slicing ACSF (below 4 °C), then recovered at 27 °C in standard ACSF (in mM; 124 NaCl, 5 KCl, 1.25 NaH_2PO_4, 26 $NaHCO_3$, 10 D-glucose, 2.5 $CaCl_2$ and 1.5 $MgCl_2$) for 1 h before recording. Slices were placed in a recording chamber, submerged, and continuously perfused (2–3 ml/min) with oxygenated standard ACSF at 27 °C. fEPSPs were recorded through low impedance (2.5–3.5 MΩ) glass micropipettes filled with standard ACSF and placed onto the CA1 SR area. Test stimuli were applied at 0.05 Hz. Stimulus intensity was determined by constructing an input–output relationship plotting the fEPSP slopes against stimulus intensities and then adjusted to 50–60% of the maximum fEPSP slope. After acquiring at least 20 min of stable fEPSP responses, 100 Hz (1 train of 100 stimuli for 1 s), 10 Hz (1 train of 100 stimuli for 10 s) or 1 Hz (3 trains of 300 stimuli for 300 s, with 300 s intervals) electrical stimuli were delivered through a tungsten bipolar electrode placed on the SR. The fEPSP slopes were analysed using WinLTP software.

The PPR was measured by pairing electrical stimuli onto the SR with inter-stimulus intervals of 20, 50 or 100 ms. Stimulus intensity was determined by constructing an input–output relationship plotting the fEPSP slopes against stimulus intensities and then adjusted to 30–40% of the maximum fEPSP slope. After acquiring at least 20 min of stable fEPSP responses, PPR was measured and calculated by dividing the

slope of the second postsynaptic response by the first one. Magnitudes of synaptic potentiation or depression elicited by 100, 10, or 1 Hz stimulation were calculated by averaging the fEPSP slopes during 40–50 min after stimulation and divided by average fEPSP slopes during baseline periods, being expressed as the percentage of the baseline average. Post-tetanic potentiation was calculated by averaging the slopes of fEPSPs for the first 5 min of recording immediately after LTP induction (100 Hz stimuli) and expressed as a percentage of the baseline average. The area of 100 Hz stimulation was measured by cumulative responses from the start of the stimulus to the zero-converging point. Amplitude refers to the first peak of the response generated by 100 Hz stimulation. Area and amplitude of 100 Hz stimulation were normalized to the mean baseline slope. Area and amplitude were analysed using Clampfit 11.0.3.

Novel object recognition and location test

The NOL test was performed in a square arena (non-glossy acrylic box, 300 × 300 × 280 mm, $W \times D \times H$, custom-made). One side has a stripe pattern to facilitate location identification. The task procedure consists of three phases: habituation, learning and test phases. Before learning, mice were habituated to the testing environment by allowing them to freely explore the open field arena for 5 min. During the learning phase, mice were placed in the open field arena containing two identical objects (A + A), for 5 min. In the test, one of the objects was moved to a new location (A + A′).

For the NOR test, the mice were also placed in a cylindrical arena (non-glossy acrylic box, 30 cm in diameter, 28 cm high). In the same manner, mice were placed in the arena for 5 min during habituation and learning phases. One of two objects (A + A) was substituted by a novel one (A + B).

During NOL or NOR tests, mice were considered to be exploring an object when the muzzle was touching or in close proximity to the object. Time spent exploring familiar and novel or displaced objects was recorded separately to calculate the discrimination ratio by dividing the difference in exploration time for the displaced or novel object by total exploration time.

Software and statistical analysis

For acquiring confocal images, the Zen (Zeiss) software acquisition system was used. For image analysis, ImageJ (NIH) and its plugins (for example, Diana) were used. For reconstructing stacked confocal images into 3D structure, IMARIS (Bitplane) was used. For acquiring TEM and SEM images, Tecnai User Interface software (FEI control imaging software) and ZEISS Atals 5 software (Gemini 300 SEM) were used.

All statistical analyses were performed using GraphPad Prism 7 with 95% confidence. Most of the imaging data when comparing two groups were analysed using a Mann–Whitney test. In the case of imaging data comparing more than three groups, one-way or two-way ANOVA followed by Tukey's multiple comparisons test was used. For ssTEM, TEM, SEM, electrophysiology and behavioural data, unpaired Student's *t*-tests were used to test significance between two groups. The statistical test used for each experiment is reported in the results. All statistic tests were two-sided. All experiments were duplicated or triplicated with similar results.

Reporting summary

Further information on research design is available in the Nature Research Reporting Summary linked to this paper.

Data availability

All primary antibodies used in this study are listed in the Methods. Recipes for reporters used in this study are provided in the Methods. All data are available upon reasonable request. For further inquiries, please contact the corresponding author. Source data are provided with this paper.

Code availability

All codes used are available upon reasonable request.

28. Fischer, D., Bieber, T., Li, Y., Elsässer, H. P. & Kissel, T. A novel non-viral vector for DNA delivery based on low molecular weight, branched polyethylenimine: effect of molecular weight on transfection efficiency and cytotoxicity. *Pharm. Res.* **16**, 1273–1279 (1999).
29. Guo, P. et al. A simplified purification method for AAV variant by polyethylene glycol aqueous two-phase partitioning. *Bioengineered* **4**, 103–106 (2013).
30. Gibson, D. G. et al. Enzymatic assembly of DNA molecules up to several hundred kilobases. *Nat. Methods* **6**, 343–345 (2009).
31. Choi, J. H. et al. Optimization of AAV expression cassettes to improve packaging capacity and transgene expression in neurons. *Mol. Brain* **7**, 17 (2014).
32. Gilles, J. F., Dos Santos, M., Boudier, T., Bolte, S. & Heck, N. DiAna, an ImageJ tool for object-based 3D co-localization and distance analysis. *Methods* **115**, 55–64 (2017).
33. Bloss, E. B., Cembrowski, M. S., Karsh, B., Fetter, R. D. & Spruston, N. Single excitatory axons form clustered synapses onto CA1 pyramidal cell dendrites. *Nat. Neurosci.* **21**, 353–363 (2018).
34. Vandael, D., Borges-Merjane, C., Zhang, X. & Jonas, P. Short-term plasticity at hippocampal mossy fiber synapses is induced by natural activity patterns and associated with vesicle pool engram formation. *Neuron* **107**, 509–521.e7 (2020).
35. Rosenmund, C. & Stevens, C. F. Definition of the readily releasable pool of vesicles at hippocampal synapses. *Neuron* **16**, 1197–1207 (1996).

Acknowledgements We thank all members of the Chung, Mun, and Park laboratories for helpful discussions, and C. Cho for reading the paper. This work was supported by grants from the Samsung Science & Technology Foundation (SSTF-BA1701-18, W.-S.C.), the National Research Foundation of Korea (NRF) (2019R1A2C1010634 (J.Y.M.), 2016M3C7A1905391), and the KBRI basic research program (20-BR-01-04 (H.P.), 20-BR-01-09 (J.Y.M)) funded by the Ministry of Science and ICT. J.-H.L is partly supported by the Global PhD Fellowship Program through the NRF funded by the Ministry of Education (2017H1A2A1042287). Instruments (SEM and TEM) and whole-cell patch clamp data were acquired at the Brain Research Core Facilities in KBRI. Imaris software was supported by Bio Core facilities in KAIST.

Author contributions W.-S.C. and H.P. designed projects. J.-H.L. designed DNA constructs used in this paper, produced AAV-based reporters, performed all imaging and western blot experiments, and analysed data. J.-Y.K. performed and analysed electrophysiology and behavioral experiments. H.L. performed and analysed electrophysiology experiments. J.-H.L. and S.N. prepared brain samples for TEM and SEM experiments. S.N. and J.Y.M. performed and analysed TEM, ssTEM and SEM experiments. S.Y.L. performed stereotaxic surgeries and analysed the phagocytic capacity of aged astrocytes. W.-S.C. and H.P. supervised the project and wrote the paper.

Competing interests The authors declare no competing interests.

Additional information

Supplementary information is available for this paper at https://doi.org/10.1038/s41586-020-03060-3.

Correspondence and requests for materials should be addressed to H.P. or W.-S.C.

Peer review information *Nature* thanks Marc Freeman, Jeremy Kay and the other, anonymous, reviewer(s) for their contribution to the peer review of this work.

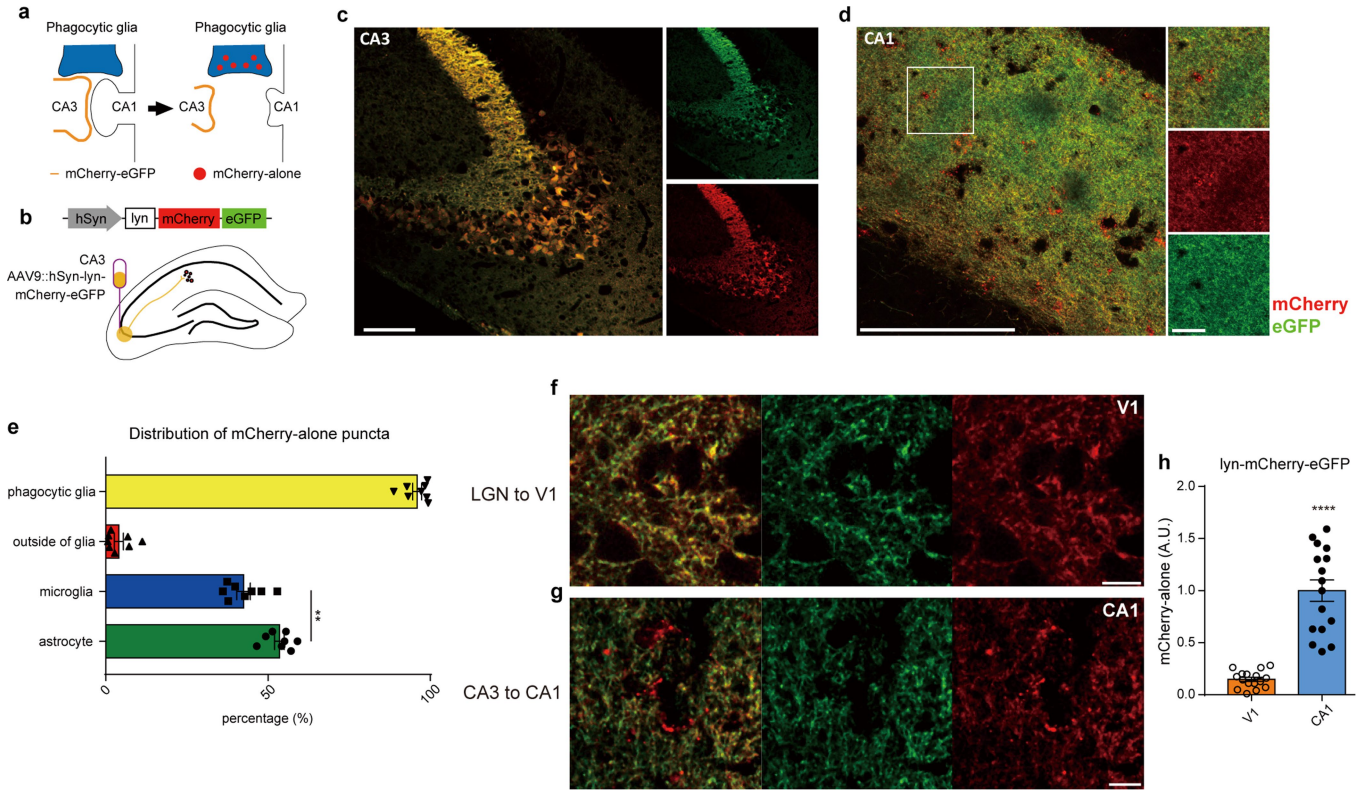

Extended Data Fig. 1 | Development of the mCherry-eGFP reporter system for monitoring glial phagocytosis. a, Schematic diagram of the mCherry-eGFP reporter system for monitoring glial phagocytosis of neuronal material. **b**, AAV9::hSyn-lyn-mCherry-eGFP was injected into hippocampal CA3 of 4-week-old mice. **c**, **d**, Representative confocal single-plane images of CA3 (**c**) and CA1 (**d**) of AAV9::hSyn-lyn-mCherry-eGFP injected mice. The white box in **d** highlights mCherry-alone puncta region. Scale bars = 100 µm (left and middle) and 10 µm (right). **e**, Distribution of mCherry-alone puncta in CA1 of AAV9::hSyn-lyn-mCherry-eGFP injected mice. $n = 8$ individual experiments from 3 mice for each group. Data are mean ± s.e.m. Astrocytes versus microglia, $^{**}P = 0.0019$. Mann–Whitney test. **f**, Representative confocal single-plane images of the primary visual cortex (V1) of the mice injected with AAV9::hSyn-lyn-mCherry-eGFP into the lateral geniculate nucleus (LGN) which projects their axons to V1. **g**, Representative confocal single-plane images of CA1 of the mice injected with AAV9::hSyn-lyn-mCherry-eGFP into CA3. Scale bars = 10 µm (**f**, **g**). **h**, Quantification of the area of mCherry-alone puncta in V1 and CA1. $n = 16$ individual experiments from 4 mice per each group. CA1 versus V1, $^{****}P < 0.0001$. For all quantified data, Mann–Whitney test. All data are mean ± s.e.m.

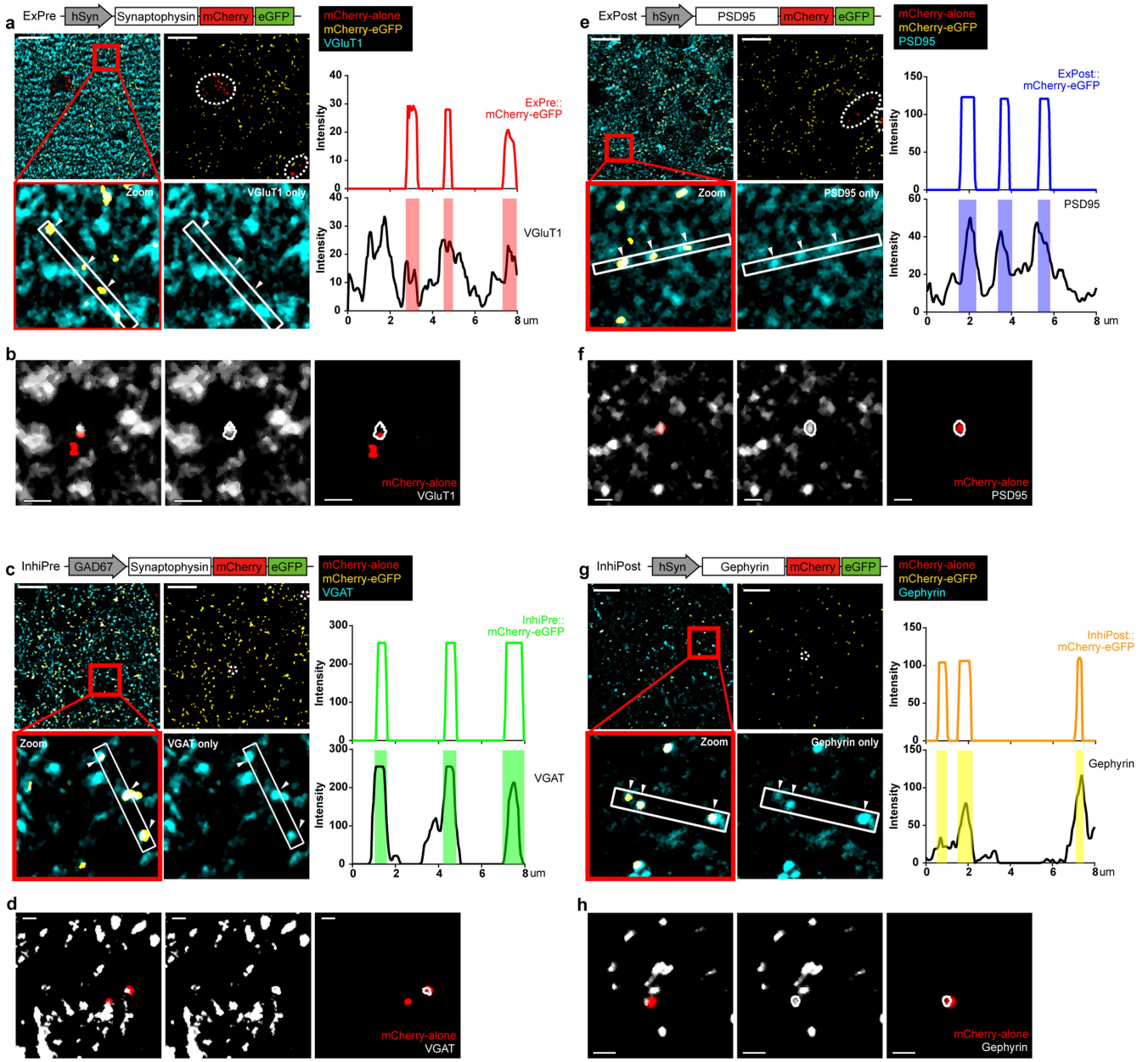

Extended Data Fig. 2 | AAV-based synapse phagocytosis reporters accurately incorporate into excitatory and inhibitory synapses. **a**, **c**, **e**, **g**, Representative confocal single-plane images of the CA1 hippocampus injected with AAV9::ExPre (**a**), AAV9::InhiPre (**c**), AAV9::ExPost (**e**) or AAV9::InhiPost (**g**) reporters. Synaptic proteins (**a**: VGluT1, **c**: VGAT, **e**: PSD95, **g**: Gephyrin, cyan) with mCherry-alone (red) and mCherry-eGFP (yellow) (upper left). mCherry-alone and mCherry-eGFP without synaptic proteins (upper right). White dotted circles highlight the mCherry-alone puncta. Zoom-in panels of the upper left panels (lower left). White arrowheads in boxes indicate the mCherry-eGFP puncta co-localized with synaptic proteins. Zoom-in panels of the upper left panels without mCherry-eGFP puncta (lower right). Scale bars = 10 μm (Histogram) Fluorescence trajectory in white boxes showing co-localization of mCherry-eGFP and synaptic proteins. **b**, **d**, **f**, **h**, Representative single-plane confocal images of mCherry-alone puncta (red) and synaptic proteins (**b**: VGluT1. **d**: VGAT, f: PSD95, **h**: Gephyrin, white). White lines indicate the synaptic protein puncta co-localized with mCherry-alone puncta.

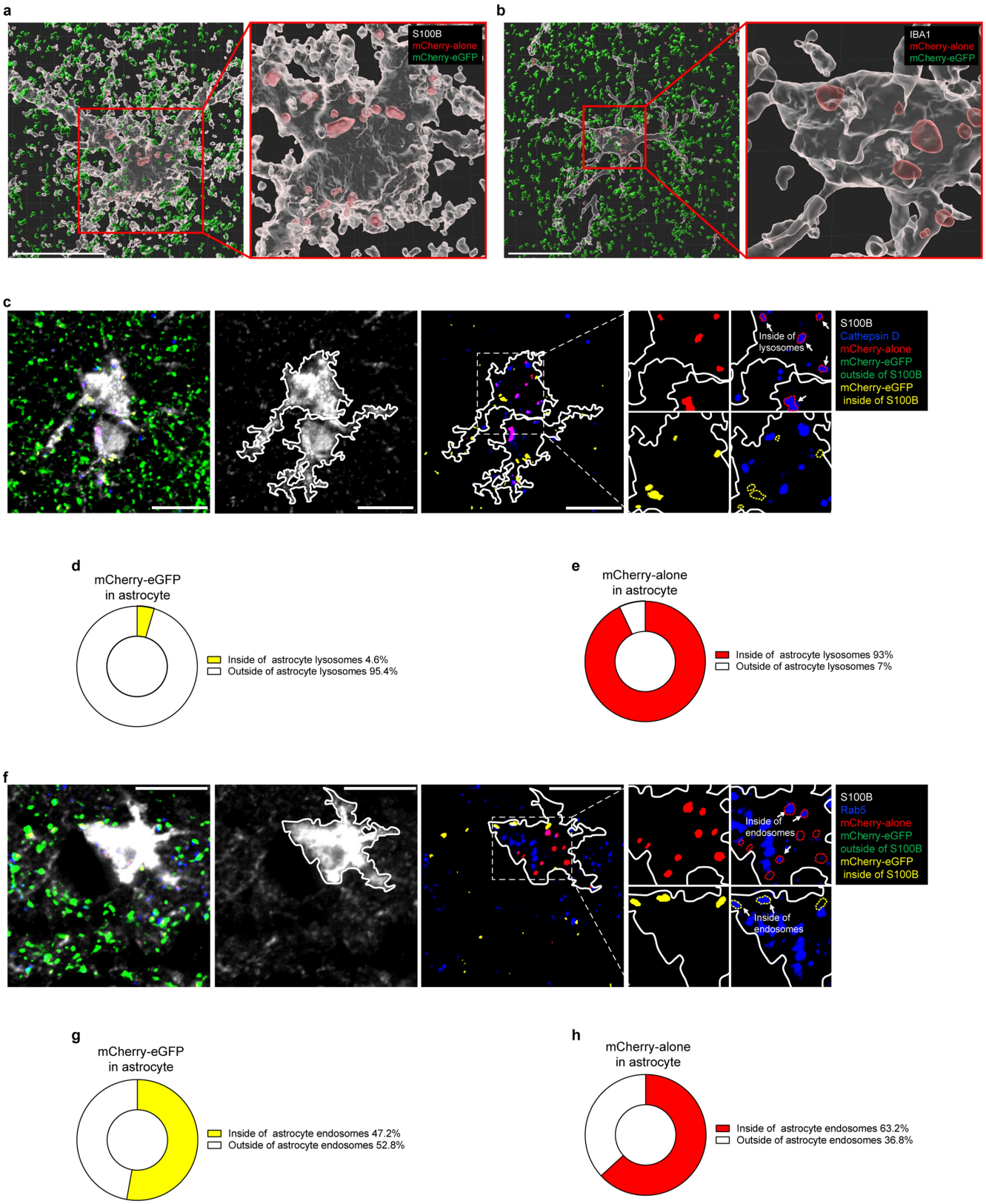

Extended Data Fig. 3 | Cellular localization of mCherry-eGFP and mCherry-alone puncta inside of glial cells. a, **b**, Representative 3D-rendered images showing ExPre-derived mCherry-alone puncta (red) and mCherry-eGFP synaptic puncta (green) associated with astrocytes (**a**, white) or microglia (**b**, white). Scale bars = 10 µm. **c**, **f**, Representative confocal single plane images showing co-localization of ExPre-derived mCherry-alone (red) or mCherry-eGFP (yellow) puncta with Cathepsin D-positive lysosomes (**c**, blue) or Rab5-positive endosomes (**f**, blue) in astrocytes (S100B, white). White lines mark the surface of astrocytes. In divided images, red and yellow dotted circles mark mCherry-alone and mCherry-eGFP puncta, respectively. White arrows indicate co-localized puncta with Cathepsin D-positive lysosomes (**c**) or Rab5-positive endosomes (**f**). Scale bars = 10 µm. **d**, **e**, **g**, **h**, Percentages of ExPre-derived mCherry-eGFP (**d**, **g**) or mCherry-alone (**e**, **h**) in either inside or outside of Cathepsin D-positive lysosomes (**d**, **e**) or Rab5-positive endosomes (**g**, **h**) in astrocytes. *n* = 3 mice per each group.

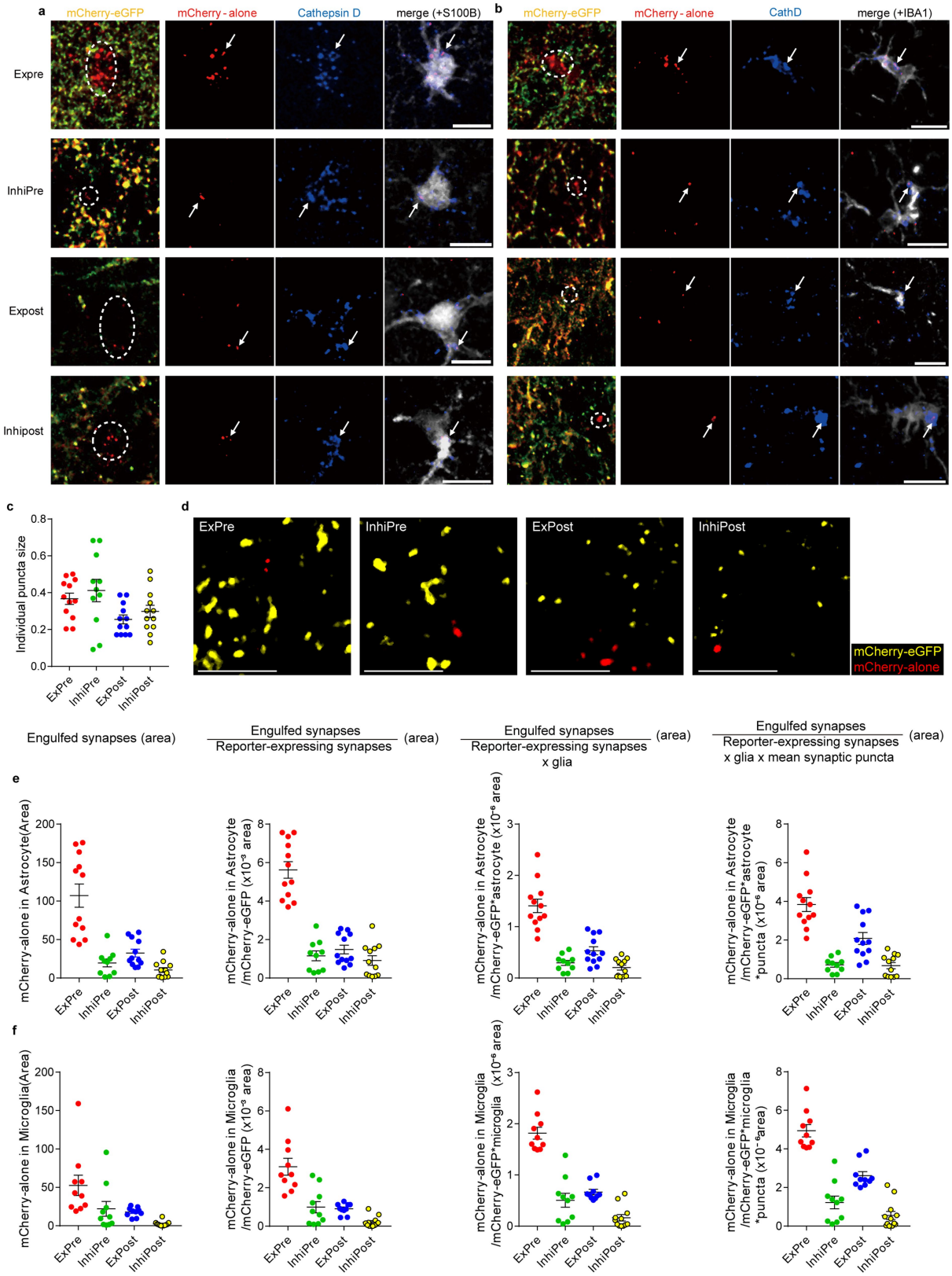

Extended Data Fig. 4 | See next page for caption.

Extended Data Fig. 4 | mCherry-alone puncta derived from glial synapse elimination reporters. a, **b**, Representative confocal z projection images of glial synapse elimination reporters (mCherry (red) and eGFP (green) derived from ExPre, InhiPre, ExPost and InhiPost), lysosome marker Cathepsin D (blue) and glial cell markers (**a**, S100B for astrocytes. **b**, IBA1 for microglia, white). Scale bars = 10 μm. White dotted circles mark mCherry-alone puncta. White arrows indicate mCherry-alone puncta co-localized with Cathepsin D inside either astrocytes (**a**) or microglia (**b**). **c**, Quantification of individual synaptic reporter puncta size (mCherry-eGFP puncta, area). *n* = 12 individual experiments per each group. **d**, Representative confocal single plane images of CA1 showing mCherry-eGFP (green) and mCherry-alone (red) puncta derived from each reporters. Scale bars = 5 μm. **e**, **f**, Detailed procedures explaining how the area of engulfed synapses (mCherry-alone) by astrocytes (**e**, *n* = 12, 10, 12, 12) or microglia (**f**, *n* = 10, 10, 10, 12) was normalized. For description, please see the Method section. For all comparisons, statistics were not applied in these graphs. For all data, each n represent individual experiment from 3 mice. All data are mean ± s.e.m.

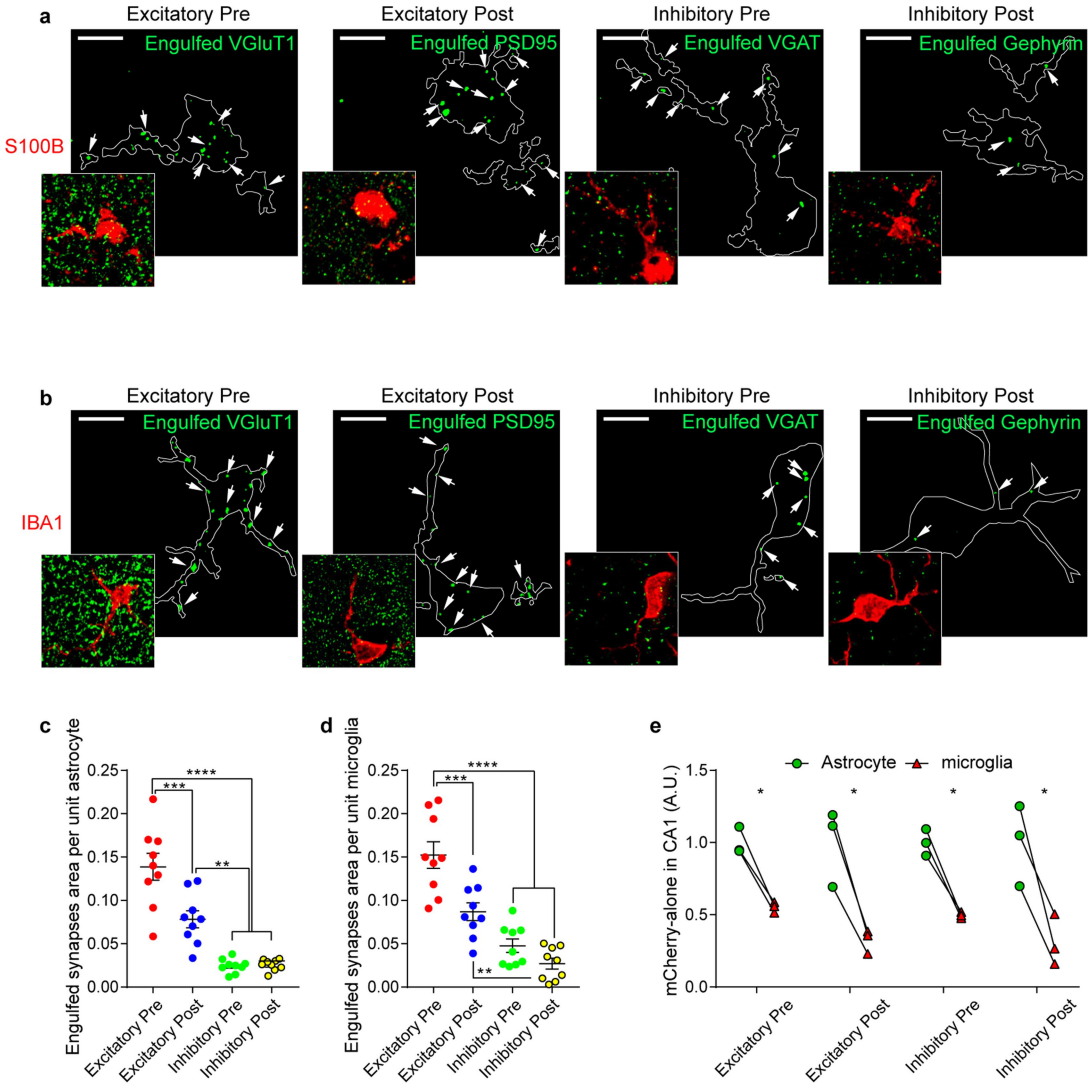

Extended Data Fig. 5 | Both astrocytes and microglia engulf more excitatory than inhibitory synapses. a, **b**, Representative confocal single plane images of CA1 astrocytes (**a**, S100B, red) or microglia (**b**, IBA1, red) with synaptic proteins (VGluT1, PSD95, VGAT or Gephyrin, green). White arrows indicate engulfed synaptic proteins in glial cells. Scale bars = 5 µm. **c**, **d**, Quantification of engulfed synaptic proteins per unit astrocytes (**c**) or microglia (**d**). $n = 9$ individual experiments from 3 mice per each groups. (**c**) Excitatory Pre versus Inhibitory Pre/Post, $^{****}P < 0.0001$. Excitatory Pre versus Excitatory Post, $^{***}P = 0.0004$. Excitatory Post versus Inhibitory Pre/Post, $^{**}P = 0.0015/0.0048$. (**d**) Excitatory Pre versus Inhibitory Pre/Post, $^{****}P < 0.0001$. Excitatory Pre versus Excitatory Post, $^{***}P = 0.0006$. Excitatory Post versus Inhibitory Post, $^{**}P = 0.0016$. One-way ANOVA followed by Tukey's multiple comparisons. **e**, Comparison between the quantified engulfed synapses by astrocytes and microglia. Excitatory Pre, $^{*}P = 0.0151$. Excitatory Post, $^{*}P = 0.0256$. Inhibitory Pre, $^{*}P = 0.0142$. Inhibitory Post, $^{*}P = 0.0428$. Mann–Whitney test. $n = 3$ mice per group. All data are mean ± s.e.m.

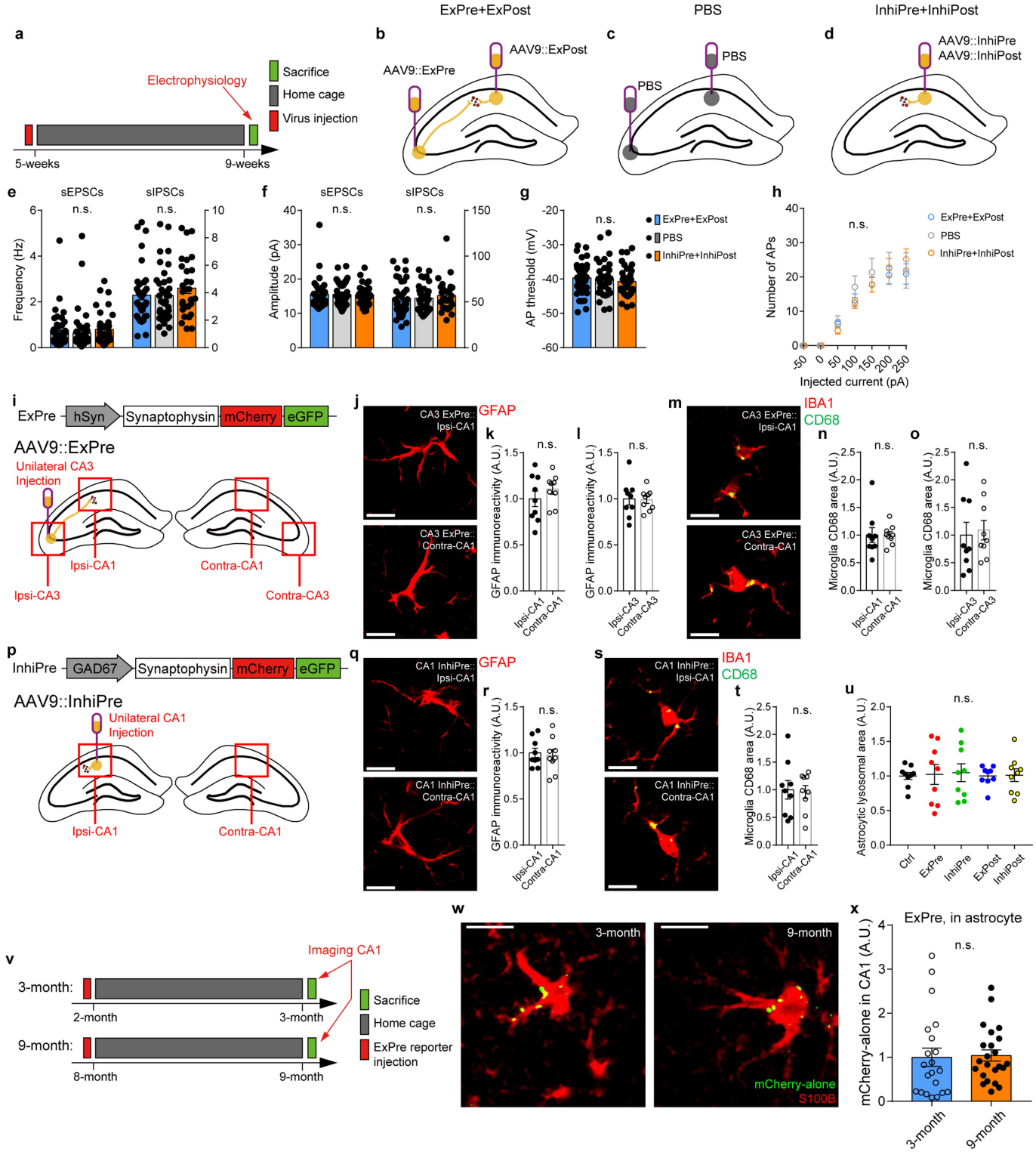

Extended Data Fig. 6 | See next page for caption.

Extended Data Fig. 6 | AAV-based synapse phagocytosis reporters do not induce changes in synaptic properties or reactive gliosis. a, Schematic diagram of experimental schedule for measuring sEPSCs and sIPSCs of reporter-expressing neurons. **b**–**d**, Representative images that depict experimental and control groups. (**b**) AAV9::ExPre and AAV9::ExPost were injected into CA3 and CA1, respectively. (**c**) PBS was injected into CA3 and CA1. (**d**) AAV9::InhiPre and AAV9::InhiPost were injected into CA1. **e**, **f**, Quantifications of mean frequencies (**e**) or amplitudes (**f**) of sEPSC/sIPSCs from ExPre+ExPost injected (**b**; sEPSC: 39 cells from 4 mice, sIPSC: 36 cells from 4 mice), PBS injected (**c**; sEPSC: 46 cells from 4 mice, sIPSC: 38 cells from 4 mice) or InhiPre+InhiPost injected (**d**; sEPSC: 37 cells from 4 mice, sIPSC: 29 cells from 4 mice) groups. **g**, Quantifications of mean voltage thresholds for action potential initiation (AP threshold) from each group. ExPre+ExPost injected: 46 cells from 2 mice, PBS injected: 36 cells from 3 mice, InhiPre+InhiPost injected: 51 cells from 3 mice. n.s. **h**, Quantifications of mean number of action potential induced by current injection in each group. ExPre+ExPost injected: 46 cells from 2 mice, PBS injected: 36 cells from 3 mice, InhiPre+InhiPost injected: 51 cells from 3 mice. One-way ANOVA followed by Tukey's multiple comparisons test (**e**–**h**). **i**, AAV9::ExPre was injected into CA3 unilaterally. After 4 weeks of recovery, ipsilateral CA3, CA1 (Ipsi-CA3, Ipsi-CA1) and contralateral CA3, CA1 (Contra-CA3, Contra-CA1) were examined. **j**, Representative confocal single plane images of GFAP expression (red) in Ipsi-CA1 (upper) or Contra-CA1 (lower) of AAV9::Expre-CA3 injected brains. **k**, **l**, Quantification of GFAP immunoreactivity comparing Ipsi- and Contra-CA1 (**k**) or CA3 (**l**). $n = 9$ individual experiments from 3 mice per each groups. Mann–Whitney test. **m**, Representative confocal single plane images of CD68 (green) expression with microglia (IBA1, red) in Ipsi-CA1 (upper) or Contra-CA1 (lower) of AAV9::Expre-CA3 injected brains. **n**, **o**, Quantification of microglial CD68 area comparing Ipsi- and Contra-CA1 (**n**) or CA3 (**o**). $n = 9$ individual experiments from 3mice per each groups. Mann–Whitney test. **p**, AAV9::InhiPre was injected into CA1 unilaterally. After 4 weeks of recovery, ipsilateral CA1 (Ipsi-CA1) and contralateral CA1 (Contra-CA1) were examined. **q**, Representative confocal single plane images of GFAP expression (red) in Ipsi-CA1 (upper) or Contra-CA1 (lower) of AAV9::Inhipre-CA1 injected brains. **r**, Quantification of GFAP immunoreactivity comparing Ipsi- and Contra-CA1. $n = 9$ individual experiments from 3 mice per each groups. Mann–Whitney test. **s**, Representative images of CD68 (green) expression with microglia (IBA1, red) in Ipsi-CA1 (upper) or Contra-CA1 (lower) of AAV9::Inhipre-CA1 injected brains. **t**, Quantification of microglial CD68 area comparing Ipsi- and Contra-CA1. $n = 9$ individual experiments from 3 mice per each groups. Mann–Whitney test. **u**, Quantification of Cathepsin D-positive lysosome area in astrocytes of control (Ctrl), AAV9::ExPre, InhiPre, ExPost and InhiPost injected brain. $n = 9$ individual experiments from 3 mice per each groups. One-way ANOVA followed by Tukey's multiple comparisons. **v**, Schematic diagram of experimental schedule for comparing the amount of engulfed excitatory pre-synapses by CA1 astrocytes in 3- and 9-month-old mice. **w**, Representative confocal single plane images of astrocytes (S100B, red) containing mCherry-alone puncta (green) in CA1 of 3- and 9-month-old mice. **x**, Quantification of the area of mCherry-alone puncta in astrocytes normalized with the area of mCherry-eGFP and astrocytes in CA1 of ExPre injected 3- and 9-month-old mice. $n = 21, 23$ from 4 mice for each group. Mann–Whitney test. For all analyses, n.s., not significant. Scale bars = 10 μm. For all comparisons, n.s., not significant. All data are mean ± s.e.m.

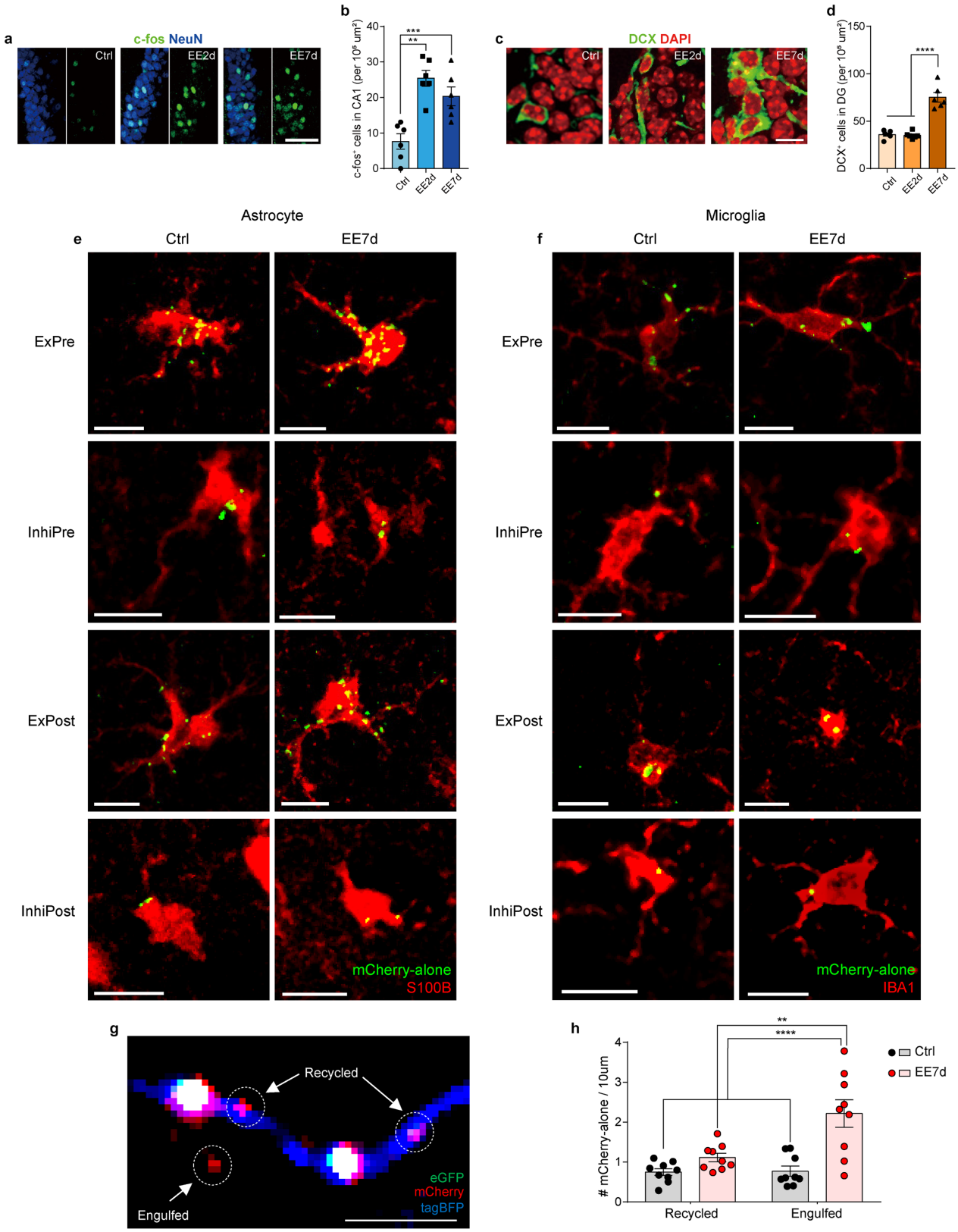

Extended Data Fig. 7 | See next page for caption.

Extended Data Fig. 7 | Hippocampal activity regulates astrocytic synapse elimination. a, Representative confocal z projection images of CA1 neurons (NeuN, blue) with c-fos (green) from Ctrl, EE2d and EE7d mice. Scale bar = 50µm. **b**, Quantification of c-fos$^+$ and NeuN$^+$ neurons in CA1 from control, EE2d and EE7d mice, $n = 6$ individual experiments from 3 mice per each group. Ctrl versus EE2d, $^{**}P = 0.0046$, Ctrl versus EE7d, $^{***}P = 0.0002$. One-way ANOVA followed by Tukey's multiple comparisons test. **c**, Representative confocal z projection images of dentate gyrus (DG) cells (DAPI, red pseudo-colored) with newborn cells (DCX, green) from Ctrl, EE2d and EE7d mice. Scale bar = 10 µm. **d**, Quantification of DCX+ cells in DG from Ctrl, EE2d and EE7d mice, $n = 6$ individual experiments from 3 mice per each group. Ctrl or EE2d versus EE7d, $^{****}P < 0.0001$. One-way ANOVA followed by Tukey's multiple comparisons test. **e**, **f**, Representative confocal single plane images of astrocytes (e, red) or microglia (f, red) containing mCherry-alone puncta (green) in CA1 of reporter-injected Ctrl and EE7d mice. Scale bars = 10 µm. **g**, A representative confocal z projection of an axon terminal labelled with ExPre reporter (synaptic boutons, yellow) and tagBFP (axon, blue) in CA1 of reporter-electroporated Ctrl mice. White dotted circles and arrows highlight mCherry-alone puncta (red) outside (engulfed) or inside (recycled) of tagBFP-positive axon terminal. Scale bar = 5 µm. **h**, Quantification of the number of mCherry-alone puncta outside (engulfed) or inside (recycled) of tagBFP-positive axon terminal in Ctrl or EE7d groups. $n = 9$ individual experiments from 5 mice per each group. EE7d engulfed versus Ctrl recycled or engulfed, $^{****}P < 0.0001$. EE7d engulfed versus EE7d recycled, $^{**}P = 0.0020$. Two-way ANOVA followed by Tukey's multiple comparisons test. All data are mean ± s.e.m.

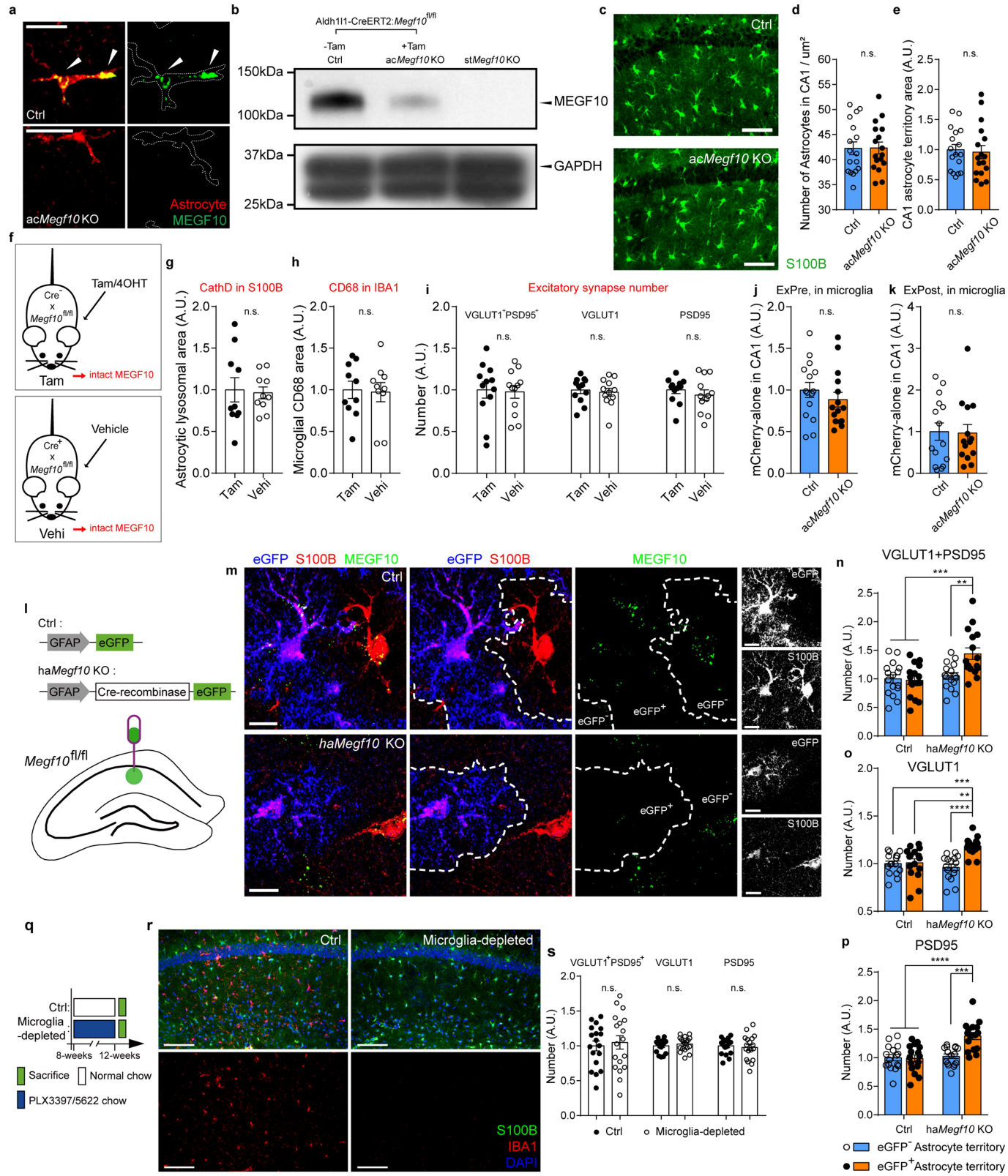

Extended Data Fig. 8 | See next page for caption.

Extended Data Fig. 8 | Astrocytes regulate nearby synapses by MEGF10 while microglia do not participate in homeostatic synapse elimination. **a**, Representative images of MEGF10 (green) with astrocytes (S100B, red) in control (upper) and ac*Megf10* KO (lower) mice. Scale bars = 20 µm. White arrowheads indicate co-localization of MEGF10 and astrocytes. **b**, western blotting of hippocampal homogenates from Ctrl, ac*Megf10* KO and straight *Megf10* KO mice. **c**, Representative confocal z projection images of astrocytes (S100B, green) in CA1 of Ctrl and ac*Megf10* KO mice. Scale bars = 60 µm. **d**, **e**, Quantification of the number (**d**) and territory area (**e**) of astrocytes in CA1 of Ctrl and ac*Megf10* KO mice. $n = 17$ individual experiments from 3 mice per each group. n.s., not significant. Mann–Whitney test. **f**, Schematic illustrations that depict the experimental and control groups. To examine potential effects in the number of excitatory synapses or glial phagocytosis, 4-hydroxytamoxifen or tamoxifen was consecutively injected into *Megf10*$^{fl/fl}$ mice without *Aldh1l1-creERT2* allele for 5 times, once per a day (Tam group). For control, vehicle (see Method) was consecutively injected into *Megf10*$^{fl/fl}$ mice with *Aldh1l1-creERT2* allele for 5 times, once per a day (Vehi group). **g**, **h**, Quantification of the area of Cathepsin D-positive lysosomes in astrocytes (**g**) or microglial CD68 (**h**) of Tam and Vehi groups. $n = 10$ individual experiments from 3 mice per each groups. $P > 0.05$. n.s., not significant. Mann–Whitney test. **i**, Quantification of the number of VGLUT1- and PSD95-double positive (left), VGLUT1-positive pre- (middle), and PSD95-positive post- (right) excitatory synapses in hippocampal CA1 of Tam and Vehi groups. $n = 12$ individual experiments from 3 mice per each group. For all comparisons, $P > 0.05$. n.s., not significant. Mann–Whitney test. **j**, **k**, Quantification of the area of mCherry-alone puncta in microglia normalized with the area of mCherry-eGFP and microglia in CA1 of AAV9::ExPre (**j**) or AAV9::ExPost (**k**) injected Ctrl and ac*Megf10* KO mice. $n = 12$ individual experiments from 4 mice for each group. n.s., not significant. Mann–Whitney test. **l**, To acquire mosaic *Megf10* KO in CA1 astrocytes, low titer of AAV5-GFAP-Cre-eGFP (ha*Megf10* KO) or AAV5-GFAP-eGFP (Ctrl) was injected into *Megf10*-floxed CA1. **m**, Representative confocal single plane images of eGFP positive (blue-colored eGFP and red-colored S100B) and negative astrocytes (S100B only), along with MEGF10 staining (green). In ha*Megf10* KO, only eGFP-positive astrocytes that express Cre fail to express MEGF10. White dotted lines mark astrocytic territories. Scale bars = 10 µm. **n**–**p**, Quantification of the number of VGLUT1- and PSD95-double positive (**n**), VGLUT1-positive pre- (**o**), and PSD95-positive post- (**p**) excitatory synapses in the eGFP-positive and negative astrocytic territories of Ctrl and ha*Megf10* KO groups. $n = 16$ individual experiments from 4 mice per each group. (n) eGFP-positive of ha*Megf10* KO versus eGFP-positive/negative of Ctrl, $^{***}P = 0.0004/0.0009$. eGFP-positive of ha*Megf10* KO versus eGFP-negative of ha*Megf10* KO, $^{**}P = 0.0039$. (**o**) eGFP-positive of ha*Megf10* KO versus eGFP-negative of Ctrl, $^{***}P = 0.0006$. eGFP-positive of ha*Megf10* KO versus eGFP-negative of ha*Megf10* KO, $^{****}P < 0.0001$. eGFP-positive of ha*Megf10* KO versus eGFP-positive of Ctrl, $^{**}P = 0.0013$. (**n**) eGFP-positive of ha*Megf10* KO versus eGFP-positive/negative of Ctrl, $^{****}P < 0.0001$. eGFP-positive of ha*Megf10* KO versus eGFP-negative of ha*Megf10* KO, $^{***}P = 0.0001$. Two-way ANOVA followed by Tukey's multiple comparisons. **q**, Schematic diagram of experimental schedule. **r**, Representative confocal z projection images of hippocampal microglia (IBA1, red) with astrocyte (S100B, green) and DAPI staining (blue), comparing control (Ctrl) and PLX3397/5622 treated (Microglia-depleted) groups. Scale bar = 100 µm. **s**, Quantification of the number of VGLUT1- and PSD95-double positive (left), VGLUT1-positive pre- (middle), and PSD95-positive post- (right) excitatory synapses in hippocampal CA1 of control and PLX3397/5622 treated mice, $n = 18$ individual experiments from 3 mice per each group. For all comparisons, $P > 0.05$. n.s., not significant. Mann–Whitney test. All data are mean ± s.e.m.

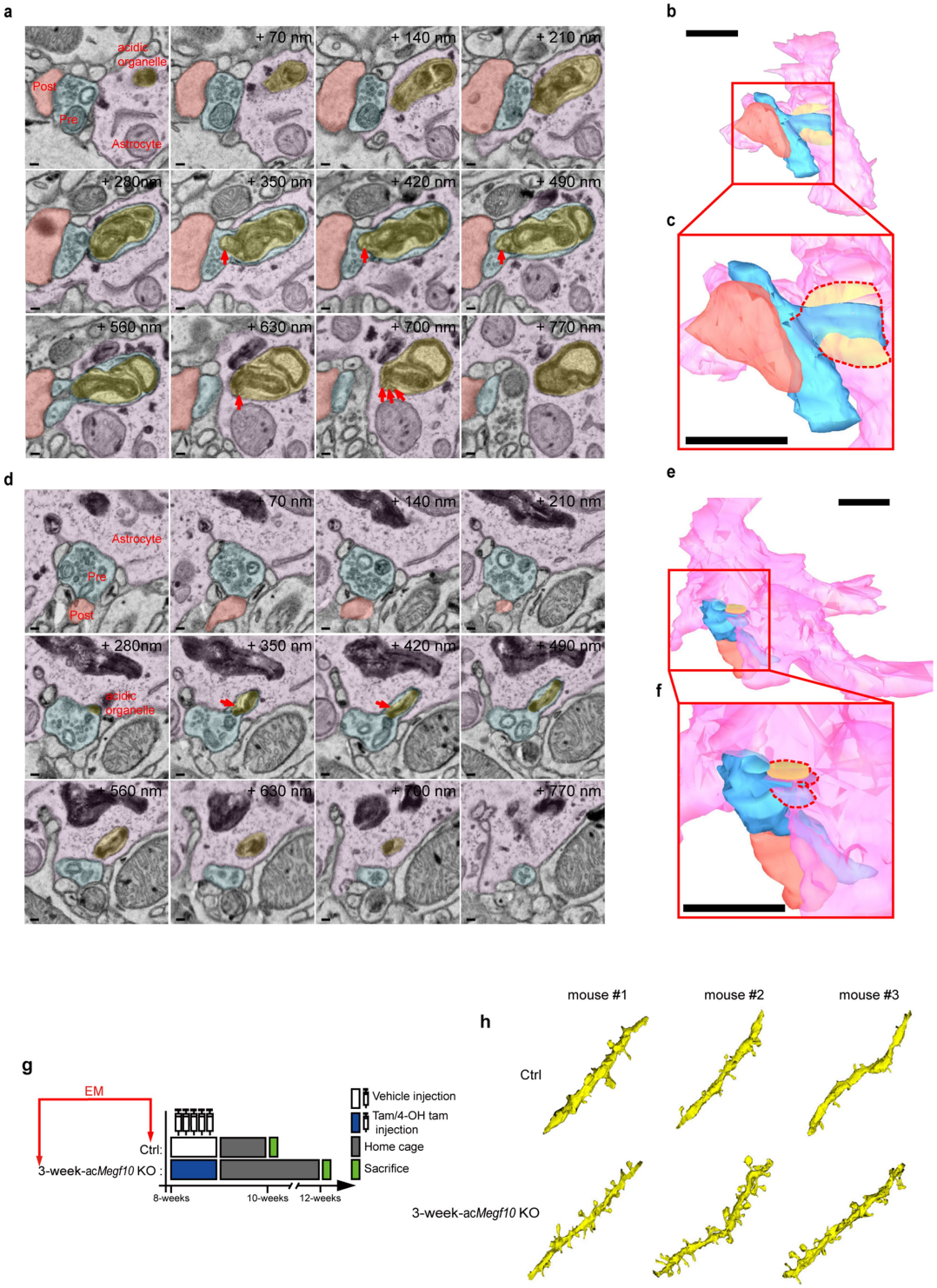

Extended Data Fig. 9 | 3-dimensional (3D) reconstruction of dendrites and astrocytes engulfing spine synapses. a–f, Representative single-plane SEM images (**a**, **d**) and 3D reconstruction of Ctrl astrocytes which are engulfing spine synapses (**b**, **c**, **e**, **f**). Scale bars = 500 nm. Red arrows indicate pre-synaptic vesicles inside of astrocytic acidic organelles. Dotted lines of 3D reconstructions highlight the synapses being engulfed and acidic organelles in astrocytes. **g**, Schematic diagram of experimental schedule. **h**, Representative images of dendrites and dendritic spines reconstructed by 3D tracing technique from Ctrl (upper), and 3-week-ac*Megf10* KO (lower) CA1 hippocampus.

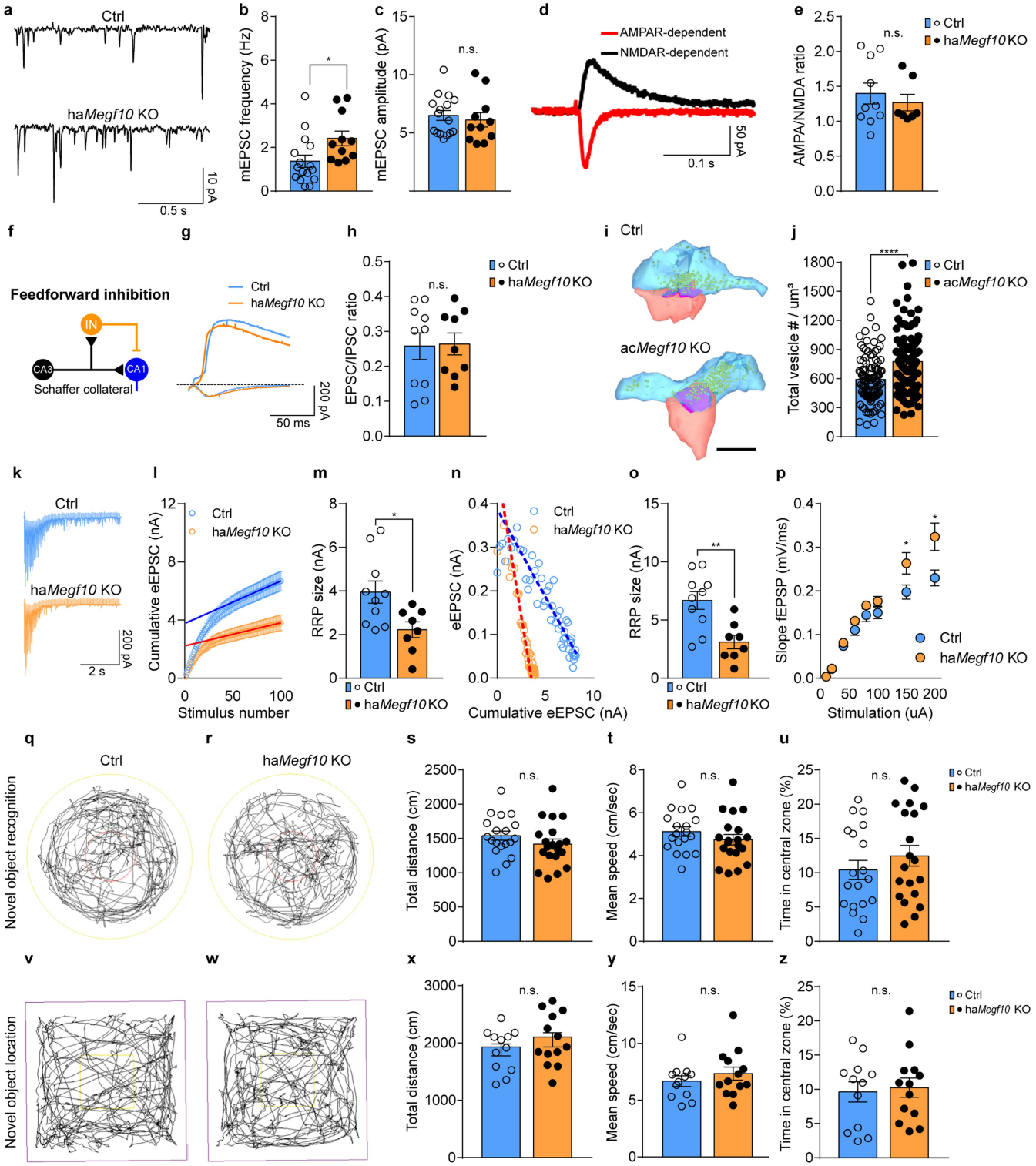

Extended Data Fig. 10 | See next page for caption.

Extended Data Fig. 10 | Synaptic properties and basal locomotive activities affected by astrocytic *Megf10* KO. a, Representative mEPSC traces recorded from control (Ctrl) or ha*Megf10* KO slices. **b**, **c**, Scatter plots showing average mEPSC frequency (b) or amplitude (c). Control (Ctrl): $n = 16$ cells from 4 mice. ha*Megf10* KO: $n = 11$ cells from 4 mice. n.s., not significant. $^{*}P = 0.0242$, unpaired Student *t*-test. **d**, Representative recording traces showing overlaid AMPAR- (red) or NMDAR-dependent evoked EPSC responses. **e**, Summary of AMPAR/NMDAR EPSC ratio (AMPA/NMDA ratio) from control (Ctrl) or ha*Megf10* KO slices. Control (Ctrl): $n = 10$ cells from 4 mice. ha*Megf10* KO: $n = 7$ cells from 3 mice. n.s., not significant. Unpaired Student *t*-test. **f**, Schematic diagram representing feed-forward inhibition circuits in the hippocampal CA1 area. **g**, Representative evoked EPSC or IPSC traces recorded from the same CA1 neuron. **h**, Bar graphs depict average EPSC/IPSC ratio from control (Ctrl) or ha*Megf10* KO slices. Control (Ctrl): $n = 10$ cells from 6 mice. ha*Megf10* KO: $n = 9$ cells from 6 mice. n.s., not significant. Unpaired Student *t*-test. **i**, Representative 3D-reconstructed EM images showing distributions of total synaptic vesicles in the hippocampus of control (Ctrl) or ac*Megf10* KO mice. Presynaptic bouton (cyan), postsynaptic spine (scarlet), postsynaptic density (purple) and synaptic vesicles (green). Scale bar = 500nm. **j**, Bar graphs depict average total vesicle numbers per μm^3. Control (Ctrl): $n = 109$ boutons from 3 mice. ac*Megf10* KO: $n = 114$ boutons from 3 mice. $^{***}P < 0.0001$, unpaired student *t*-test. **k**, Representative cumulative EPSC responses recorded from CA1 neurons in control (blue) or ha*Megf10* KO (orange), in response to 20 Hz for 5 s stimulation. **l**, Plot showing cumulative evoked EPSC (eEPSC) amplitudes during 20 Hz stimulation. Data points in a range of 4 – 5 s were fitted by linear regression, and back-extrapolated (solid line) to time 0 to estimate the RRP size (SMN method). **m**, Bar graphs depicting summary of estimated RRP size by the SMN method. Ctrl (blue): $n = 10$ cells from 3 mice; haMegf10 KO (orange): $n = 8$ cells from 3 mice. $^{*}P = 0.0181$, unpaired Student's *t*-test. **n**, Plot showing eEPSC amplitudes against the amplitude of the cumulative eEPSC in Ctrl or ha*Megf*10 KO mice. Plots were linearly fitted from the sixth to the twentieth cumulative eEPSCs and back-extrapolated linear fits to the *x* axis to estimate the RRP (EQ method). **o**, Bar graphs depicting summary of estimated RRP size by the EQ method. Ctrl (blue): $n = 10$ cells from 3 mice; ha*Megf10* KO (orange): $n = 8$ cells from 3 mice. $^{*}P = 0.0026$, unpaired Student's *t*-test. **p**, Summary of input/output relationships of fEPSP recorded from Ctrl or ha*Megf10* KO hippocampal slices, $n = 10$ and 11 slices in Ctrl and ha*Megf10* KO, respectively. $^{*}P = 0.0431$ (150 μA), $^{*}P = 0.0203$ (200 μA). Unpaired student's *t*-test. **q**, **r**, Representative traces showing mouse-travelling in the open field chamber during the NOR habituation phase in Ctrl (q) and ha*Megf10* KO mice (r). **s**–**u**, Bar graphs depict total distance (s), mean speed (t), percentage of time in central zone (u) of Ctrl and ha*Megf10* KO mice, $n = 19$ and 20 mice in Ctrl and ha*Megf10* KO, respectively. No statistical significance was found. Unpaired Student's *t*-test. **v**, **w**, Representative traces showing mouse-travelling in the open field chamber during the NOL habituation phase in Ctrl (**v**) and ha*Megf10* KO mice (**w**). **x**–**z**, Bar graphs depict total distance (**x**), mean speed (**y**), percentage of time in central zone (**z**) of Ctrl and ha*Megf10* KO mice, $n = 12$ and 13 mice in Ctrl and ha*Megf10* KO, respectively. No statistical significance was found. Unpaired Student's *t*-test. All data are mean ± s.e.m.

nature research

Corresponding author(s): 2020-03-03731A

Last updated by author(s): Oct 21th, 2020

Reporting Summary

Nature Research wishes to improve the reproducibility of the work that we publish. This form provides structure for consistency and transparency in reporting. For further information on Nature Research policies, see Authors & Referees and the Editorial Policy Checklist.

Statistics

For all statistical analyses, confirm that the following items are present in the figure legend, table legend, main text, or Methods section.

n/a	Confirmed	
☐	☒	The exact sample size (*n*) for each experimental group/condition, given as a discrete number and unit of measurement
☐	☒	A statement on whether measurements were taken from distinct samples or whether the same sample was measured repeatedly
☐	☒	The statistical test(s) used AND whether they are one- or two-sided *Only common tests should be described solely by name; describe more complex techniques in the Methods section.*
☒	☐	A description of all covariates tested
☐	☒	A description of any assumptions or corrections, such as tests of normality and adjustment for multiple comparisons
☒	☐	A full description of the statistical parameters including central tendency (e.g. means) or other basic estimates (e.g. regression coefficient) AND variation (e.g. standard deviation) or associated estimates of uncertainty (e.g. confidence intervals)
☒	☐	For null hypothesis testing, the test statistic (e.g. *F*, *t*, *r*) with confidence intervals, effect sizes, degrees of freedom and *P* value noted *Give P values as exact values whenever suitable.*
☒	☐	For Bayesian analysis, information on the choice of priors and Markov chain Monte Carlo settings
☒	☐	For hierarchical and complex designs, identification of the appropriate level for tests and full reporting of outcomes
☒	☐	Estimates of effect sizes (e.g. Cohen's *d*, Pearson's *r*), indicating how they were calculated

Our web collection on statistics for biologists contains articles on many of the points above.

Software and code

Policy information about availability of computer code

Data collection	ZEN software (ZEISS Image acquisition software, v2.3), Tecnai User Interface software (FEI control imaging software, v4.6.4), ZEISS Atlas 5 software (v5.2.3.1), SmartSEM (v6.06)
Data analysis	Image J (NIH, v1.52g) and its plugin (e.g. Diana, TrakEM2 plug-in), IMARIS (Bitplane, v9.2), GraphPad Prism (v7.0) EM image reconstruct software (https://synapseweb.clm.utexas.edu/software-0).

For manuscripts utilizing custom algorithms or software that are central to the research but not yet described in published literature, software must be made available to editors/reviewers. We strongly encourage code deposition in a community repository (e.g. GitHub). See the Nature Research guidelines for submitting code & software for further information.

Data

Policy information about availability of data

All manuscripts must include a data availability statement. This statement should provide the following information, where applicable:

- Accession codes, unique identifiers, or web links for publicly available datasets
- A list of figures that have associated raw data
- A description of any restrictions on data availability

Full list of primary antibodies used in this study are in method sections. Recipes for reporters used in this study are in method sections. All data and code are available upon reasonable request. For further inquiries, please contact Corresponding author.

Field-specific reporting

Please select the one below that is the best fit for your research. If you are not sure, read the appropriate sections before making your selection.

☒ Life sciences ☐ Behavioural & social sciences ☐ Ecological, evolutionary & environmental sciences

For a reference copy of the document with all sections, see nature.com/documents/nr-reporting-summary-flat.pdf

Life sciences study design

All studies must disclose on these points even when the disclosure is negative.

Sample size	For imaging experiments, predetermination of sample sizes was not performed. Sample sizes were chosen as standard in the field. The animal numbers were based on estimation from previous studies, including our own published studies (Chung et al, Nature 2013).
Data exclusions	For imaging analysis, Data were excluded out based on outliers test (Grubbs' test, 95% confidence) supplied by GraphPad. For eletrophysiology experiment, individual cases that did not meet proper cell properties criteria were exclude (cells with unstable access resistance >20% change). Also, in behavior experiments, mice that did not meet the sample session criteria was excluded from analysis (at least 10 s of total sample object exploration).
Replication	Experiments were repeated, and the results are reproducible. Electrophysiology, imaging and behavioral studies were conducted using different cohorts of animals. The outcomes are consistent, and results are robust.
Randomization	Mice were randomly assigned to experimental vs. control groups with matched age and sex, whenever possible. brain sections used for imaging were selected randomly.
Blinding	During the experiment and analysis, all experiments were performed blindly.

Reporting for specific materials, systems and methods

We require information from authors about some types of materials, experimental systems and methods used in many studies. Here, indicate whether each material, system or method listed is relevant to your study. If you are not sure if a list item applies to your research, read the appropriate section before selecting a response.

Materials & experimental systems

n/a	Involved in the study
☐	☒ Antibodies
☐	☒ Eukaryotic cell lines
☒	☐ Palaeontology
☐	☒ Animals and other organisms
☒	☐ Human research participants
☒	☐ Clinical data

Methods

n/a	Involved in the study
☒	☐ ChIP-seq
☒	☐ Flow cytometry
☒	☐ MRI-based neuroimaging

Antibodies

Antibodies used	Rabbit anti-S100b (Abcam, ab52642, 1:1000), rabbit anti-IBA1 (Wako, 019-19741, 1:500), Chicken anti-GFAP (Abcam, ab4674, 1:500), goat anti-Cathepsin D (R&D systems, AF1029, 1:500), guinea pig anti-VGAT (Synaptic systems, 131 003, 1:500), guinea pig anti-VGluT1 (Millipore ab5095, 1:2000), rabbit anti-c-Fos (Cell signaling, 2250S, 1:500), rabbit anti-DCX (Doublecortin, Abcam, ab18723, 1:500), mouse anti-NeuN (Millipore, MAB377, 1:500), rabbit anti-MEGF10 (Millipore, ABC10, 1:500), rabbit anti-PSD95 (Invitrogen, 51-6900, 1:500), rabbit anti-Gephyrin (synaptic systems, 147 008, 1:500), chicken anti-GFP (Aves labs, GFP-1020, 1:1000), goat anti-IBA1 (Novus, NB100-1028, 1:500), rat anti-RFP (for mCherry, Chromotek, 5F8, 1:500), rat anti-mCherry (Invitrogen, M11217, 1:500), rabbit anti-DsRED (Clontech, 632496, 1:200), rabbit anti-tRFP (for tagBFP, Evrogen, AB233, 1:500), rabbit anti-Rab5 (Abcam, ab18211, 1:500), guinea pig anti-S100B (Synaptic systems, 287 004 1:500), rat anti-CD68 (Bio-Rad, MCA1957, 1:500). Donkey anti-Rabbit IgG (H+L) Alexa Fluor 594 (invitrogen, A21207, 1:500), Donkey Anti-Rabbit IgG (H+L) Alexa Fluor 405 (Abcam, ab175649, 1:200), Donkey anti-Rabbit IgG (H+L) Alexa Fluor 647 (invitrogen, A31573, 1:200), Donkey anti-Rabbit IgG (H+L) Alexa Fluor 488 (invitrogen, A21206, 1:1000), Goat anti-Chicken IgY (H+L) Alexa Fluor 488 (invitrogen, A11039, 1:1000), Donkey Anti-Goat IgG (H+L) Alexa Fluor 405 (Abcam, ab175665, 1:200), Donkey anti-Mouse IgG (H+L) Alexa Fluor 488 (invitrogen, A21202, 1:1000), Donkey anti-Rat IgG (H+L) Alexa Fluor 594 (invitrogen, A21209, 1:500), Donkey anti-Guinea Pig IgG (H+L) Alexa Fluor 594 (Jackson lab, 706-585-148, 1:500), Goat anti-guinea pig IgG (H+L) Alexa Fluor 405 (abcam, ab175678, 1:200)
Validation	Rabbit anti-S100b (Abcam) : supported by several references including PubMed: 30478038 rabbit anti-IBA1 (Wako) : supported by several references including PubMed: 24270812 Chicken anti-GFAP (Abcam) : supported by several references including PubMed: 11138011

goat anti-Cathepsin D (R&D systems) : supported by several references including PubMed: 25874770
guinea pig anti-VGAT (Synaptic systems) : Verified through KO experiments by manufacturer
guinea pig anti-VGluT1 (Millipore) : supported by several references including PubMed: 25807484
rabbit anti-c-Fos (Cell signaling) : supported by several references including PubMed: 31805115
rabbit anti-DCX (Doublecortin, Abcam) : supported by several references including PubMed: 30770803
mouse anti-NeuN (Millipore) : supported by several references including PubMed: 26373451
rabbit anti-MEGF10 (Millipore) : Verified through western blot experiment by manufacturer
rabbit anti-PSD95 (Invitrogen) : Verified through western blot experiments by manufacturer
rabbit anti-Gephyrin (synaptic systems) : Verified through KO experiments by manufacturer
chicken anti-GFP (Aves labs) : supported by several references including PubMed: 30808661
goat anti-IBA1 (Novus) : supported by several references including PubMed: 31270459
rat anti-RFP (for mCherry : Chromotek) : supported by several references including PubMed: 18642673
rat anti-mCherry (Invitrogen) : Verified through western blot and IHC experiments by manufacturer
rabbit anti-DsRED (Clontech) : Verified through western blot and IHC experiments by manufacturer
rabbit anti-tRFP (for tagBFP, Evrogen) : Verified through western blot and IHC experiments by manufacturer
rabbit anti-Rab5 (Abcam): supported by several references including PubMed: 30962435
guinea pig anti-S100B (Synaptic systems): supported by several references including PubMed: 31340158
rat anti-CD68 (Bio-Rad): supported by several references including PubMed: 26139610

Donkey anti-Rabbit IgG (H+L) Alexa Fluor 594
Donkey Anti-Rabbit IgG (H+L) Alexa Fluor 405
Donkey anti-Rabbit IgG (H+L) Alexa Fluor 647
Donkey anti-Rabbit IgG (H+L) Alexa Fluor 488
Goat anti-Chicken IgY (H+L) Alexa Fluor 488
Donkey Anti-Goat IgG (H+L) Alexa Fluor 405
Donkey anti-Mouse IgG (H+L) Alexa Fluor 488
Donkey anti-Rat IgG (H+L) Alexa Fluor 594
Donkey anti-Guinea Pig IgG (H+L) Alexa Fluor 594
Goat anti-guinea pig IgG (H+L) Alexa Fluor 405

All stated secondary antibodies were verified through IHC experiment by manufacturer

Eukaryotic cell lines

Policy information about cell lines

Cell line source(s)	HEK293T
Authentication	None of the cell lines used were authenticated
Mycoplasma contamination	None of the cell lines used were not tested for mycoplasma contamination
Commonly misidentified lines (See ICLAC register)	unregistered, HEK293T cells were utilized to produce AAV vectors

Animals and other organisms

Policy information about studies involving animals; ARRIVE guidelines recommended for reporting animal research

Laboratory animals	For Imaging, electrophysiology and EM experiments, Mus musculus (C57/BL6) were used. Genders were not considered. The mice were sacrificed at the age of 9 weeks to 12 weeks. For behavior experiments, all mice used were the C57BL/6J background strains of either male or female at 8-14 weeks old. Megf10 fl/fl mice (8-14 weeks) were used for slice electrophysiology and behavior experiments.
Wild animals	No wild animals were used in this study
Field-collected samples	No field-collected samples were used in this study
Ethics oversight	All mouse experiments were performed according to articles approved by Institutional Animal Care and Use Committees (IACUC) protocols from Korea Advanced Institute of Science and Technology (KAIST) and Korea Brain Research Institute (KBRI).

Note that full information on the approval of the study protocol must also be provided in the manuscript.